

# The impact of multidecadal Atlantic meridional overturning circulation variations on the Southern Ocean

Liping Zhang<sup>1,2</sup> · Thomas L. Delworth<sup>2</sup> · Fanrong Zeng<sup>2</sup>

Received: 11 August 2015 / Accepted: 20 May 2016 / Published online: 31 May 2016  
© Springer-Verlag Berlin Heidelberg 2016

**Abstract** The impact of multidecadal variations of the Atlantic meridional overturning circulation (AMOC) on the Southern Ocean (SO) is investigated in the current paper using a coupled ocean–atmosphere model. We find that the AMOC can influence the SO via fast atmosphere teleconnections and subsequent ocean adjustments. A stronger than normal AMOC induces an anomalous warm SST over the North Atlantic, which leads to a warming of the Northern Hemisphere troposphere extending into the tropics. This induces an increased equator-to-pole temperature gradient in the Southern Hemisphere (SH) upper troposphere and lower stratosphere due to an amplified tropical upper tropospheric warming as a result of increased latent heat release. This altered gradients leads to a poleward displacement of the SH westerly jet. The wind change over the SO then cools the SST at high latitudes by anomalous northward Ekman transports. The wind change also weakens the Antarctic bottom water (AABW) cell through changes in surface heat flux forcing. The poleward shifted westerly wind decreases the long term mean easterly winds over the Weddell Sea, thereby reducing the turbulent heat flux loss, decreasing surface density and therefore leading to a weakening of the AABW cell. The weakened AABW cell produces a temperature dipole in the SO, with a warm anomaly in the subsurface and a cold anomaly in the surface that corresponds to an increase of Antarctic sea ice. Opposite conditions occur for a weaker than normal AMOC.

Our study here suggests that efforts to attribute the recent observed SO variability to various factors should take into consideration not only local process but also remote forcing from the North Atlantic.

**Keywords** Atlantic meridional overturning circulation · Southern Ocean · Antarctic sea ice

## 1 Introduction

The Atlantic meridional overturning circulation (AMOC) plays a crucial role in the global climate system, characterized by a northward flow of warm and salty water in the upper layer of the Atlantic, and a southward flow of cold water in the deep Atlantic (e.g. Bryden et al. 2005; Wunsch and Heimbach 2006). The AMOC transports a large amount of heat from the Southern Hemisphere (SH) and tropics to the North Atlantic where the heat is released to the atmosphere (e.g. Delworth et al. 2008). This AMOC-induced anomalous northward heat transport favors generating a north–south sea surface temperature (SST) dipole across the Atlantic equator (e.g. Delworth et al. 1993; Zhang and Delworth 2005; Knight et al. 2005; Wu et al. 2008; Zhang and Wang 2013), which is frequently used to explain the Atlantic multidecadal oscillation (AMO) (e.g. Folland et al. 1984; Gray et al. 1997; Delworth and Mann 2000; Wang and Zhang 2013; Zhang and Wang 2013).

Changes in the AMOC have a profound impact on the Northern Hemispheric and tropical climate system. Paleoclimate records and North Atlantic waterhosing experiments showed that a weakening of AMOC is associated with colder than normal temperature over Europe and the U.S., a southward shift of the Atlantic intertropical convergence zone (ITCZ) as well as decreased Indian/Sahel

✉ Liping Zhang  
Liping.Zhang@noaa.gov

<sup>1</sup> Atmospheric and Oceanic Science, Princeton University, Princeton, NJ, USA

<sup>2</sup> NOAA/Geophysical Fluid Dynamics Laboratory, 201 Forrestal Rd., Princeton, NJ 08540, USA

precipitation and Atlantic hurricane activity (e.g. Black et al. 1999; Peterson et al. 2000; Vellinga et al. 2002; Zhang and Delworth 2005; Stouffer et al. 2006; Wu et al. 2008). The AMOC change induces significant responses outside the Atlantic as well, including the tropical Pacific El Niño–Southern Oscillation (ENSO) (e.g. Dong and Sutton 2002; Timmermann et al. 2005; Dong and Sutton 2007), summer Asian and Indian monsoon (Wang et al. 2001; Altabet et al. 2002), river runoff to the Cariaco Basin (Wang et al. 2004), and North Pacific temperature (Timmermann et al. 2007; Wu et al. 2008; Zhang and Delworth 2005). In contrast, few studies focused on the impact of AMOC on the SH, particularly on the Southern Ocean (SO).

The impact of AMOC on the SH is commonly related to the bipolar seesaw in temperature anomalies (e.g. Crowley 1992; Stocker et al. 1992; Knight et al. 2005; Stouffer et al. 2007; Delworth and Zeng 2012). It is argued that changes in the strength of the AMOC would lead to warming of one hemisphere while the other cools due to the anomalous northward heat transport. This out of phase relationship between the temperature in the North Atlantic and Antarctic is also revealed by many indirect proxy records (e.g. Blunier and Brook 2001; Broecker 1998, 2000; Weaver et al. 2003). Broecker (1998, 2000) hypothesized that these paleoclimate bipolar seesaw phenomena reflect an alternation of deep formation in the two hemispheres, where an enhanced North Atlantic deep water (NADW) formation leads to a weakened Antarctic bottom water (AABW) formation and vice versa. Based on a simple paleoclimate model, Weaver et al. (2003) verified that a weakening of AABW by freshening the southern high latitudes could lead to a switch of the AMOC from an “off” to an “on” state. Stouffer et al. (2007) and Swingedouw et al. (2009) further pointed out that the SO freshwater initially triggers a spin up of the AMOC in a realistic climate model, however, the freshwater can spread to the North Atlantic region several decades later, eventually leading to a spin down of the AMOC. Stouffer et al. (2007) also suggested that the North Atlantic freshwater input that leads to a weakening of the AMOC produces a slight warming in the SH, but has little impact on the AABW formation. Latif et al. (2013) and Martin et al. (2013) demonstrated that the SO deep water convection and SST have their own centennial internal variability that is independent of other internal variability and forced response, which contribute some to the recent decadal trends observed in the SH. This internal variability may be superimposed on the AMOC-triggered AABW variability, which could offset the potential effect of AMOC on the AABW to some extent. Therefore, whether the AMOC influences the AABW or not is still not clear yet, particularly in the current climate.

Here we use a fully coupled climate model Geophysical Fluid Dynamics Laboratory (GFDL) CM2.1 (Delworth

et al. 2006) with fixed preindustrial forcing to comprehensively study the SO response to the multidecadal AMOC variations. In addition to surface air temperature and SST that were addressed by previous studies (e.g. Zhang and Delworth 2005; Stouffer et al. 2006, 2007), we specifically pay attention to the SO subsurface temperature, deep water formation, wind driven circulation, and sea ice change induced by the AMOC. We attempt to address by which path the multidecadal AMOC variations can influence the SO and what the potential mechanisms are behind this influence. We also try to address to what extent recently observed SO variability can be attributed to the AMOC influence.

The paper is organized as follows. Section 2 briefly describes the coupled model, sensitivity experiments design, observational datasets as well as reanalysis data. The simulated SO response to the multidecadal AMOC fluctuations is presented in Sect. 3. Possible mechanisms controlling the SO response to the multidecadal AMOC are examined in Sect. 4. In Sect. 5, we investigate the potential linkages of recent SO cooling with the AMOC. Discussion and summary are given in Sect. 6.

## 2 Model description, experimental design and datasets

The coupled model used in this study is Geophysical Fluid Dynamics Laboratory (GFDL) CM2.1 (Delworth et al. 2006). The atmospheric model has a horizontal resolution of  $2.5^\circ$  in longitude and  $2.0^\circ$  in latitude, with 24 levels in the vertical. The horizontal resolution of the ocean model is  $1^\circ$  in the extratropics, with finer meridional grid-spacing in the tropics ( $\sim 1^\circ/3^\circ$ ). The ocean model has 50 levels in the vertical, with 22 evenly spaced levels over the top 220 m. The coupled model runs for 2000-year with atmospheric constituents and external forcing held constant at 1860.

We wish to assess how the SO responds to multidecadal AMOC variations. Here we use an idealized 100-year periodic North Atlantic Oscillation (NAO, Hurrell 1995) forcing to trigger multidecadal AMOC variations. Previous studies have pointed out that the NAO can lead to significant responses in the AMOC (e.g. Delworth and Dixon 2000; Lohmann et al. 2009), with a positive (negative) NAO phase corresponding to a spin up (spin down) of AMOC. The positive NAO-related fluxes, mainly the heat flux, tend to extract more heat from the North Atlantic Ocean, thereby cooling and increasing the density of the upper ocean and thus leading to a strengthening of the AMOC and vice versa. The anomalous NAO forcing used in this study comes from the ECMWF-Interim reanalysis (Dee et al. 2011), as well as the time series of the observed NAO using a station-based index (downloaded from the

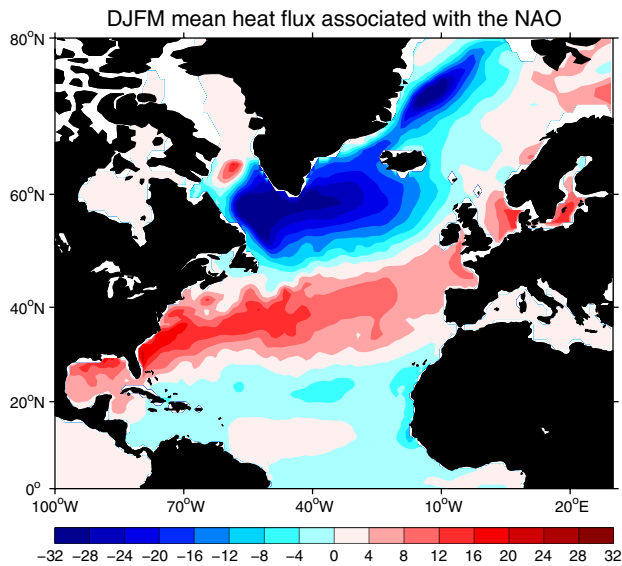


**Fig. 1** Spatial pattern of the heat flux anomalies ( $\text{W/m}^2$ , positive downward) used as anomalous flux forcing in the model experiments. The flux is calculated from the ECMWF-Interim reanalysis, and is the mean flux over December–March that corresponds to one standard deviation of the North Atlantic Oscillation in observation

NCAR/UCAR climate data guide at <https://climatedata-guide.ucar.edu/climate-data/hurrell-north-atlantic-oscillation-nao-index-station-based>). We compute 4-month averages over the December–March period. Figure 1 shows the regression map for surface heat flux anomalies associated with a one standard deviation increase in the NAO. The anomalous heat flux forcing is only over the North Atlantic from the equator to  $82^\circ\text{N}$ , including the Barents and Nordic Seas. The area integral of the heat flux is constrained to be zero, so that there is no net addition of heat to the system.

The coupled model normally computes air-sea fluxes of heat, water and momentum that depend on the gradients in these quantities across the air-sea interface. In our perturbation experiment this process continues, but after these fluxes are calculated we add an additional flux component to the model ocean. The model ocean therefore “feels” the fluxes that are computed based on air-sea gradients, plus an extra flux that corresponds to an idealized NAO heat flux which has the spatial pattern in Fig. 1 and has the amplitude modulated sinusoidally in time with a 100-year period. The NAO forcing is applied only in the months of December through March, with a linear taper at the start and end of this period. It is worth noting that the idealized NAO-forcing used here is not the only way to trigger multidecadal AMOC variation and the same purpose can be accomplished if we use 100-year periodic freshwater forcing.

In brief, we conduct two parallel ten-member ensembles of simulations, with each simulation extending for 300 years. The first ensemble is a set of control simulations,

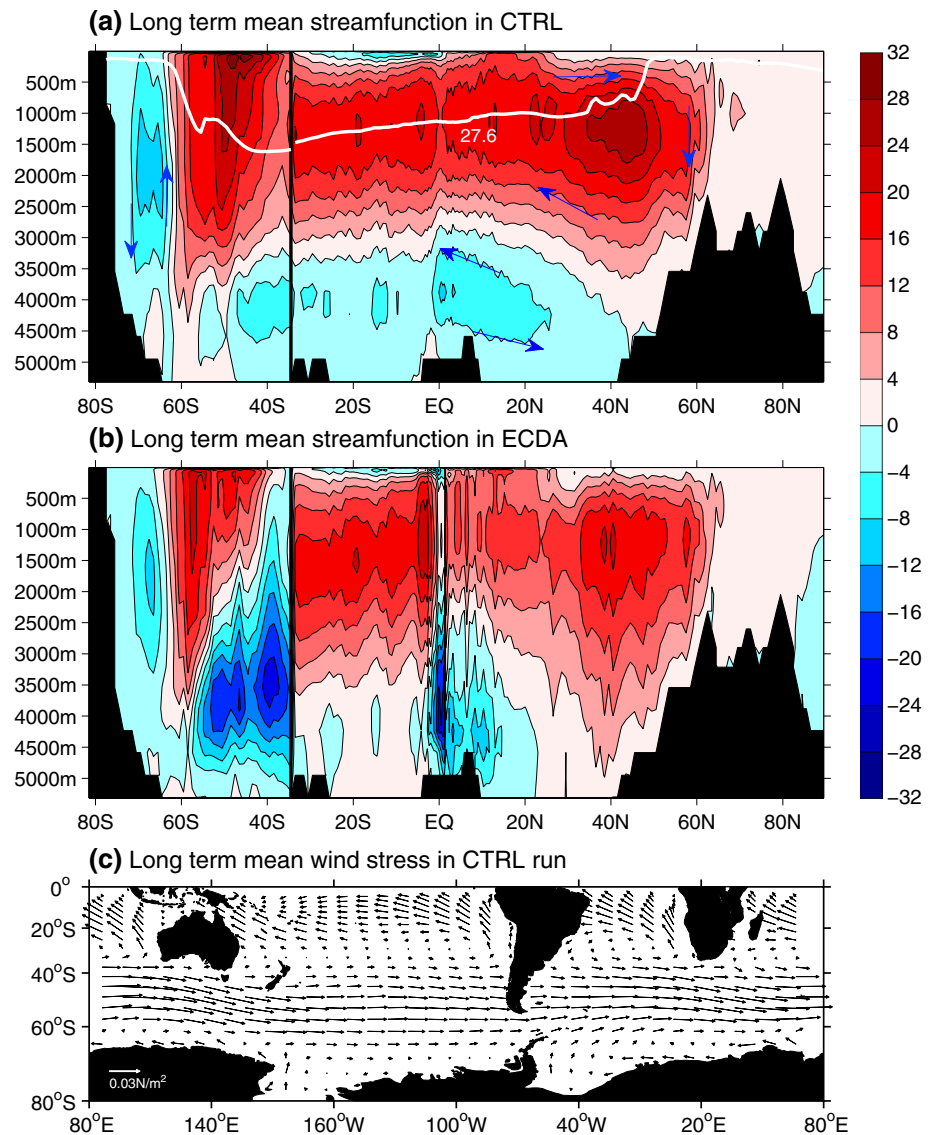
with atmospheric composition and radiative forcing fixed at preindustrial conditions. The second ensemble is identical, except that for each simulation the additional NAO-related heat flux forcing is applied to the ocean component of the model. The difference between the ensembles is interpreted as the influence of the NAO-related fluxes on the climate system. To highlight the AMOC-induced SO response rather than intrinsic variability, all results shown are ensemble means.

Several observational and reanalysis datasets are used to evaluate the model results. We use an extended reconstructed SST (ERSST) data set on a  $2^\circ \times 2^\circ$  grid from 1854 to 2013 (Smith and Reynolds 2004). We use the Hadley Centre Sea Ice and sea surface temperature data set (HadISST), available on a  $1^\circ \times 1^\circ$  grid from 1870 to 2015 (Rayner et al. 2003). We use the monthly objectively analyzed subsurface temperature data set (Ishii et al. 2006) from 1945 to 2013, which has a horizontal  $1^\circ \times 1^\circ$  grid, with 23 layers in the upper 1500 m. We also use the atmospheric reanalysis product for the twentieth century, designated as 20CRv2. The reanalysis output extends from 1871 to 2012, with output available at  $2^\circ$  spatial resolution (Compo et al. 2011). In addition, we use the ECDA reanalysis dataset (Zhang et al. 2007) that is based on an ensemble adjustment Kalman filter applied to the fully coupled GFDL CM2.1 model, in which the atmosphere is constrained by the NCEP atmospheric analysis and the ocean assimilates observations of SST from satellite and temperature and salinity from the World Ocean Database 2009 and Argo profile. The ECDA reanalysis has the same horizontal and vertical resolutions with the GFDL CM2.1. We use output from 1961 to 2013.

### 3 Simulated SO response to the multidecadal AMOC variations

Before investigating the SO response to the multidecadal AMOC change, we define some indices to represent typical circulations over the Atlantic and SO. Figure 2a shows the latitude-depth section of the long-term mean streamfunction in the fully coupled control run. Note that the streamfunction north of  $32^\circ\text{S}$  is integrated in the Atlantic Ocean, while south of  $32^\circ\text{S}$  it denotes the global streamfunction. The AMOC is characterized by a clockwise circulation, with a northward flow in the upper 1500-m and a southward flow below. Consistent with previous studies (e.g. Schmitz 1996; Swingedouw et al. 2009), the isopycnal  $27.6 \text{ kg/m}^3$  (white line in Fig. 2a) approximately corresponds to the limit between the upper and lower branches of the AMOC. Here, we define the AMOC index as the maximum streamfunction value in  $20^\circ\text{--}60^\circ\text{N}$  band and below 500-m. The depth limit is used to exclude the shallow subtropical cell

**Fig. 2** Latitude-depth section of the meridional overturning streamfunction in the Atlantic Ocean (north of 32°S) and in the Southern Ocean (south of 32°S). The contour interval is 4 Sv. *Red shading* denotes positive values representing clockwise circulation; *blue* denotes negative values representing anticlockwise circulation. Shown are the long-term mean streamfunction in the **a** fully coupled GFDL CM2.1 control run (Delworth et al. 2006) and **(b)** ECDA reanalysis (Zhang et al. 2007). The *white line* superimposed in **a** denotes the zonally averaged 27.6 kg/m<sup>3</sup> isopycnal. **c** Long-term mean surface wind stress (N/m<sup>2</sup>) in the fully coupled control simulation

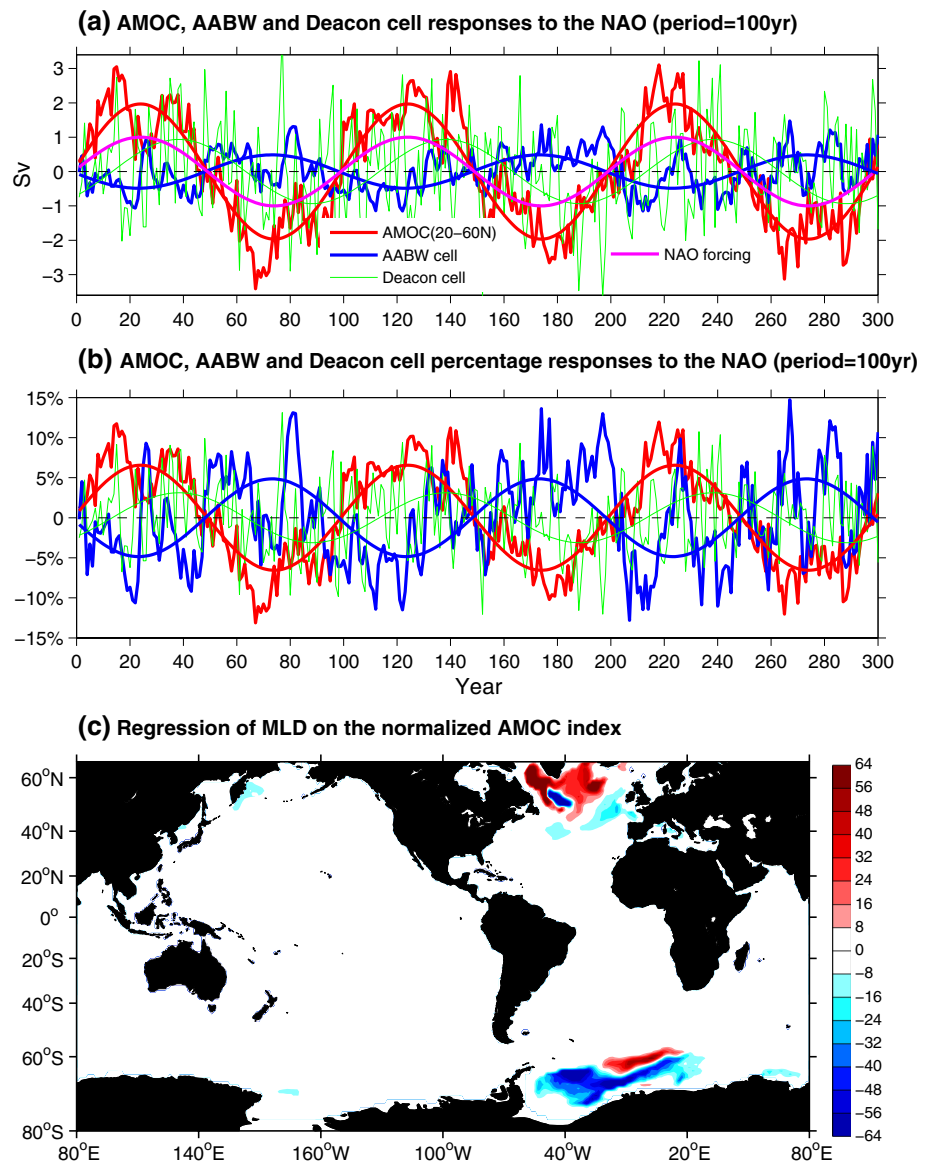


(STC) in the upper layer. In the control run, the AMOC maximum, which is located near 49.5°N and 1400-m depth, is about 26 Sv. In the SO, there is a strong clockwise MOC around the Antarctic circumpolar current (ACC) region (~40°S–60°S). In contrast to the buoyancy-driven AMOC, this meridional cell is mainly wind-driven. The prevailing westerly over the ACC region induces a northward Ekman transport in the surface, leading to a surface water divergence (convergence) south (north) of westerly. Due to mass conservation, the downwelling formatted in the convergence region tends to move southward, then upwells to the surface to compensate local water divergence and eventually generates a clockwise MOC named as Deacon Cell. The strength of Deacon Cell here is well represented by the maximum streamfunction in the 40°–60°S band. The long term mean Deacon Cell in GFDL CM2.1 control run is about 30 Sv. The streamfunction value south of 60°S is

negative (Fig. 2a), which represents a counterclockwise cell and mainly reflects the AABW formation. Here, we use the absolute value of the minimum streamfunction south of 60°S from surface to the bottom of the ocean to represent the strength of AABW. The AABW value is about 10 Sv in GFDL model using this definition, which is lower than the observed estimates ( $21 \pm 6$  Sv) suggested by Ganachaud and Wunsch (2001).

We show in Fig. 3 the AMOC, AABW and Deacon Cell responses. To focus on multidecadal variability, we also display the 30-year low pass filtered indices. Figure 3a exhibits that the low-passed AMOC index is simultaneously in phase with the NAO forcing at a time scale of 100 years, with a positive NAO corresponds to a spin up of the AMOC and vice versa. Physically, the positive (negative) NAO-related heat flux tends to extract (input) heat from (to) the ocean, thereby cooling (warming) and

**Fig. 3** **a** Annual mean extratropical AMOC (red line), AABW (blue line) and Deacon Cell (green line) responses to the 100-year periodic NAO flux forcing (magenta line). The AMOC index is defined as the maximum Atlantic streamfunction in the 20°N–60°N band and below 500-m. The AABW cell is denoted as the absolute value of the minimum global streamfunction south of 60°S. The maximum global streamfunction between 60°S and 40°S represents the strength of the Deacon Cell. Both the unfiltered and 30-year low pass filtered indexes are shown. Unit is Sv. **b** Same as **a** but for the percentage change (response divided by the long-term mean value). **c** Regression of the mixed layer depth (MLD) against the normalized 30-year low pass filtered AMOC index at lag zero. Unit is m



increasing (decreasing) the density of the upper ocean, and in turn leading to a strengthened (weakened) AMOC (e.g. Delworth and Dixon 2000; Lohmann et al. 2009). Note that the response time of the AMOC to the NAO forcing is around a decade or less (Lohmann et al. 2009; Delworth and Zeng 2016), and this adjustment time is much shorter than the forcing period (100-year). Therefore, the AMOC mainly follows the NAO forcing, without obvious time lag. In response to a one standard deviation of observed NAO variability, the multidecadal AMOC changes  $\sim 4$  Sv (peak to peak) (Fig. 3a), which accounts for  $\sim 12\%$  (peak to peak) of the long-term mean AMOC (Fig. 3b).

We now turn our attention to the SO. The deepest impression from Fig. 3a is that the AABW cell varies out of phase with the AMOC index on longer time scales, with a spin up of AMOC corresponding to a weakened AABW

formation and vice versa. We note that the real magnitude change of AABW cell ( $\sim 1.5$  Sv, peak to peak) is smaller than the AMOC response ( $\sim 4$  Sv, peak to peak, Fig. 3a). However, the percentage change of AABW cell is comparable to, sometime even higher than, the AMOC change (Fig. 3b). We can also characterize this anti-correlated relationship between the AMOC and AABW cell by the mixed layer depth change. As shown in Fig. 3c, the deepened (shoaled) mixed layer depth over the North Atlantic deep convection region (Labrador sea, Irminger sea and south Greenland) associated with a stronger (weaker) than normal AMOC coincides with a shoaled (deepened) mixed layer depth in the Weddell sea. This ocean bipolar seesaw phenomenon in the current climate is similar to the work of Broecker (1998, 2000) in the context of the paleoclimatic record. The green lines shown in Fig. 3a, b are the

wind-driven Deacon Cell response to a 100-year periodic NAO forcing. The Deacon Cell response is positively correlated with the AMOC change with a lag of several decades. This indicates that the westerly wind over the SO tends to strengthen (weaken) as the AMOC accelerates (decelerates). The time lags are mainly determined by the SST response to AMOC and slow ocean circulation adjustments to wind (will be explained in detail in Sect. 4).

The isopycnal depth variation is useful in illustrating the density driven circulation (AMOC and AABW cell) response. We plot the time evolution of Atlantic zonal mean  $27.6 \text{ kg/m}^3$  isopycnal depth anomaly at various latitudes to further show how the AMOC signal propagates and how the AABW cell responds in meridional direction (Fig. 4). In the forcing region, the spin up (down) of AMOC corresponds to a shoaling (deepening) of the  $27.6 \text{ kg/m}^3$  isopycnal (Fig. 3a vs. Fig. 4). This is because: The increased (decreased) density as the AMOC strengthens (weakens) in the whole column of North Atlantic favors an increase (a decrease) of the NADW production. This deep water mass is replaced by heavier (lighter) water in the surface layers of the ocean, which shoals (deepens) the  $27.6 \text{ kg/m}^3$  isopycnal. The shoaled (deepened) isopycnal in the northern high latitudes then propagates southward in two different speeds separated by  $35^\circ\text{N}$ . The propagation speed north of  $35^\circ\text{N}$  is very slow, while in  $35^\circ\text{N}$ – $35^\circ\text{S}$  band the speed is very fast that almost varies simultaneously in different latitudes. This latitudinal dependence of isopycnal propagation speed is an interactive product of external forced period and internal advective/wave speed inside the Atlantic Ocean. As suggested by Zhang (2010), the interior advection speed determines the AMOC propagation time north of  $35^\circ\text{N}$ . Note that this is the region where it is forced by a strong external forcing with a period of 100-year that is much longer than the internal advective time inside the Atlantic Ocean. The coupled effect of external forcing and internal advection speed in turn generates the slow propagation speed of  $27.6 \text{ kg/m}^3$  isopycnal north of  $35^\circ\text{N}$ . From the equator to  $35^\circ\text{N}$ , the propagation speed is mainly determined by the fast Kelvin wave along the western boundary (Zhang 2010), hence, the  $27.6 \text{ kg/m}^3$  isopycnal depth at various latitudes in this band are almost in phase. In the equator, the Kelvin wave moves eastward quickly and then propagates southward to the SH along the eastern boundary. In the eastern boundary, the isopycnal anomaly also spreads westward by the Rossby wave with a slower speed at higher latitudes than at lower latitudes (e.g. Johnson and Marshall 2002; Zhang 2010). Therefore, the propagation speed of  $27.6 \text{ kg/m}^3$  isopycnal depth from equator to  $35^\circ\text{S}$  is affected by both Kelvin and Rossby wave speeds.

The  $27.6 \text{ kg/m}^3$  isopycnal depth change south of  $40^\circ\text{S}$  is totally antisymmetric to that in the Northern Hemisphere (NH), with a shoaling depth in the North Atlantic coinciding with a deepening of isopycnal depth in the Weddell sea

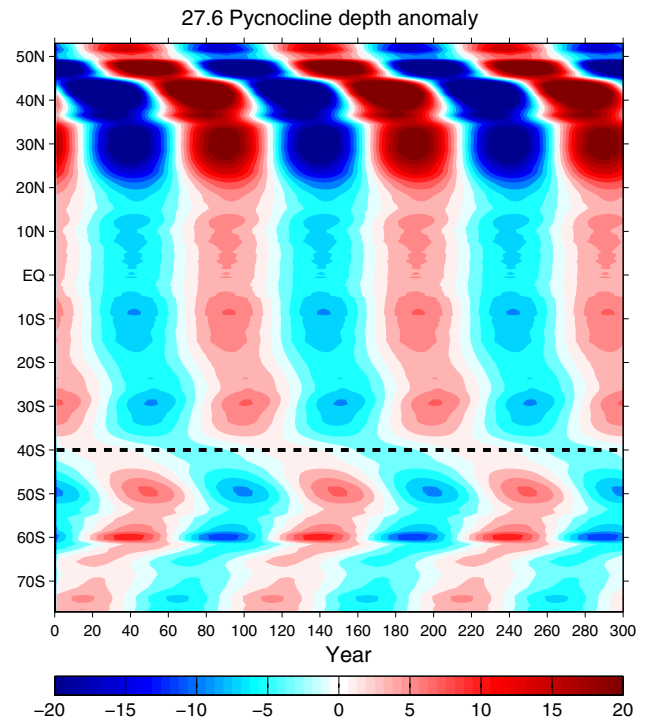


**Fig. 4** Shown are the zonally averaged ( $60^\circ\text{W}$ – $20^\circ\text{E}$ )  $27.6 \text{ kg/m}^3$  isopycnal depth response (30-year low pass filtered) to the 100-year periodic NAO flux forcing. Unit is m

and vice versa. The isopycnal deepening (shoaling) implies that the AABW formation decreases (enhances), which is largely due to the decreased (increased) density over the Weddell Sea (not shown). Similar to the North Atlantic, the high latitudinal isopycnal depth anomaly in the SH gradually propagates northward, with a forced slow advection speed south of  $45^\circ\text{S}$ . Note that the isopycnal depth anomaly over the Weddell Sea (south of  $70^\circ\text{S}$ ) lags that over the South Greenland (north of  $45^\circ\text{N}$ ) by about two decades. This implies that the AABW cell passively responds to the AMOC change or its associated climate impacts. Moreover, the isopycnal depth propagation within the SO advection band (south of  $45^\circ\text{S}$ ) takes a shorter time than that in the North Atlantic (north of  $35^\circ\text{N}$ ).

In agreement with the isopycnal depth propagation, the AMOC index shows a strong latitudinal dependence. As presented in Fig. 5, the high latitudinal AMOC index (red line) leads the relatively low latitudinal AMOC index (green line) by several years. The anomalous AMOC finally leads to significant SST anomalies over the North Atlantic due to the anomalous northward heat transport, characterized by a warm SST anomaly over the North Atlantic as the AMOC strengthens and vice versa (Fig. 5a). A close examination finds that the North Atlantic SST lags the extratropical AMOC index by several years. This lag is primarily due to the slow adjustment of ocean.

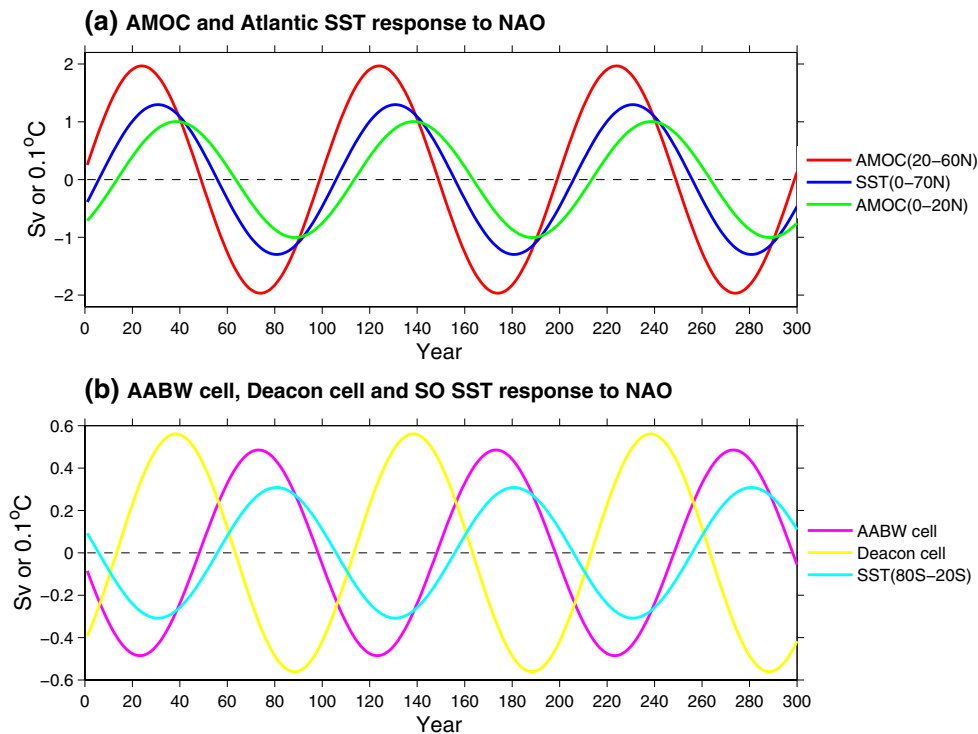


**Fig. 5** Time series of annual mean responses to the 100-year periodic NAO flux forcing. **a** Red line denotes the AMOC in the extratropical North Atlantic (20°–60°N), green line denotes the AMOC in the tropical North Atlantic (0°–20°N), and the blue line denotes the SST averaged over 0°–70°N, and from coast to coast. **b** AABW (magenta

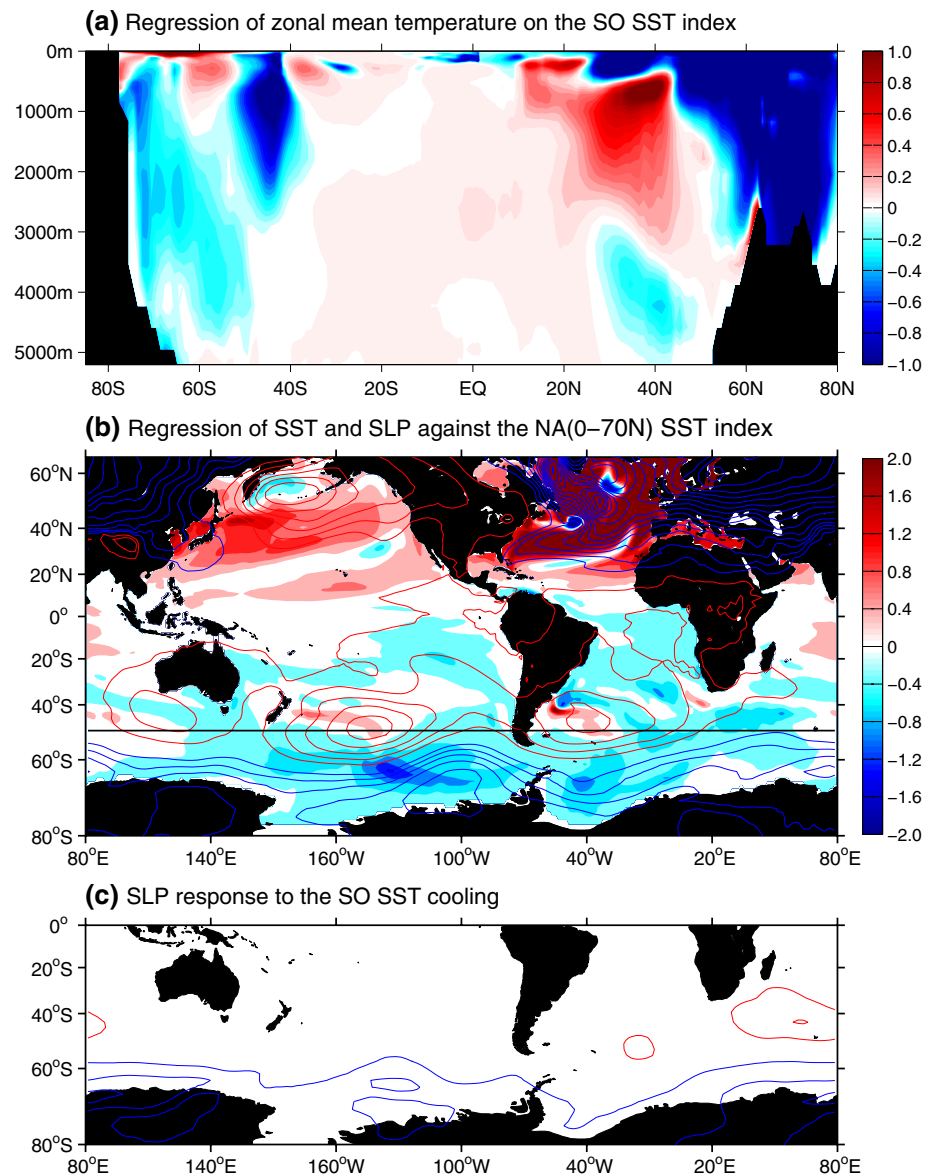
line), Deacon Cell (yellow line) and area averaged Southern Ocean (80°–20°S, coast to coast) SST (baby blue line). Units are Sv for the MOC and 0.1 °C for the SST. All data are 30-year low pass filtered to retain low frequency variability

Similar to the AMOC, the AABW variations are finally reflected in the SO temperature. Figure 5b exhibits that the AABW cell varies in phase with the SO SST but with a lead of several years. Again, this lead-lag is attributed to the ocean adjustment time. Given that the mean state of SO subsurface ocean is warmer than the surface, the stronger than normal AABW cell is in favor of entraining more subsurface warm water to the surface, which in turn generates a warm SST anomaly in the surface and a cold SST in the subsurface and vice versa. This explanation is further confirmed by the regressed zonal mean temperature pattern upon the SO SST index (Fig. 6a) that shows an obvious temperature dipole in the SO. Note that the entire NH in Fig. 6a is featured by typical AMOC fingerprints such as the tropical North Atlantic surface–subsurface temperature dipole (e.g. Zhang 2010; Wang and Zhang 2013), indicating a strong linkage between the AMOC and SO on multidecadal time scales. Due to the out of phase relationship between the AMOC and AABW cell, the SST anomalies in the North Atlantic and SO are strongly anticorrelated (Figs. 5, 6a). This inter-hemispheric dipole SST structure is more clearly seen from the regressed global SST pattern upon the North Atlantic SST index (Fig. 6b).

The SO SST anomalies could further feedback to the overlying atmosphere. We perform two sensitivity

experiments to verify this ocean feedback. The first run is control restoring experiment in which we restore (5 days restoring time scale) the model output SST at every time-step to the climatological SST seasonal cycle in control simulation over the SO (50°S–90°S, 80°E–80°W), while the ocean and atmosphere are fully active elsewhere. The other experiment is the same as the first run, but with the SST in the SO restoring to an SST field that is the sum of the seasonal cycle from the control simulation plus the SST anomaly south of 50°S derived from the regression pattern (Fig. 6b). Both runs are integrated for 50 years and the last 40 years differences are taken as the response. A 10-member ensemble run is performed with each experiment starting from an equilibrium state of a long fully coupled control simulation, and the ensemble-mean response is shown. In response to a cold SST anomaly in the SO, the sea level pressure (SLP) anomaly is characterized by a positive phase of Southern Annular Mode (SAM) and strengthened westerly winds (Fig. 6c). Note that the magnitude of SLP response is much smaller than the simultaneously regressed SLP anomaly which mainly reflects the atmosphere forcing of ocean (Fig. 6b vs. c), indicating a weak SST feedback over the SO. The enhanced westerly can amplify the initial SO cold SST anomaly via increased latent heat loss and

**Fig. 6** Spatial patterns of simulated temperature bipolar seesaw response to the 100-year periodic NAO forcing. **a** Regression of annually-averaged zonal mean ( $0^{\circ}$ – $360^{\circ}$ E) temperature response upon the 30-year low pass filtered Southern Ocean ( $90^{\circ}$ – $40^{\circ}$ S) area averaged SST index. Unit is  $^{\circ}\text{C}/^{\circ}\text{C}$ . **b** Regression of annually-averaged SST (*shading*) and SLP (*contours*, contour interval is 0.3) responses upon the 30-year low pass filtered North Atlantic ( $0^{\circ}$ N– $70^{\circ}$ N, coast to coast) area averaged SST index. Units are  $^{\circ}\text{C}/^{\circ}\text{C}$  for SST and  $\text{hPa}/^{\circ}\text{C}$  for SLP. **c** SLP response (contour interval: 0.3 hPa) to the Southern Ocean SST cooling anomaly south of  $50^{\circ}$ S in **b** which we imposed in the fully coupled model



northward Ekman transport, which in turn generates a local weak positive air-sea feedback. The enhanced westerly also leads to a spin up of the Deacon Cell after the adjustments of ocean (Fig. 5b).

We show in Fig. 7 the SO sea ice response to the NAO forcing at a time scale of 100 year. Generally speaking, the annual mean SO sea ice is increased (decreased) when the SO SST becomes cool (warm) (Fig. 7a), particularly in the Ross and Weddell seas where the deep water forms. Here, local ocean temperature is the dominant factor to determine sea ice change. The sea ice response is also somehow affected by the surface wind during the austral winter when the surface wind is strongest throughout the year. In the austral winter, the low pressure system over the Amundsen Sea is extremely low, favoring a warm air advection from subtropics to the Antarctic Peninsula region and a cold air

advection from polar Antarctic to the Ross and Amundsen seas (Fig. 7b) and vice versa. This anomalous warm/cold air advection eventually drives a weak sea ice dipole distribution displayed in Fig. 7b.

#### 4 Physical mechanisms controlling the SO response to the multidecadal AMOC variations

In this section we attempt to address what mechanisms control the ocean bipolar seesaw described above, particularly what processes determine the SO response. For this purpose, we analyze outputs of two experiments. Experiment with 100-year periodic NAO forcing is examined to derive hypothetical contributors. The second “switch on” experiment, in which we suddenly turn on and maintain an



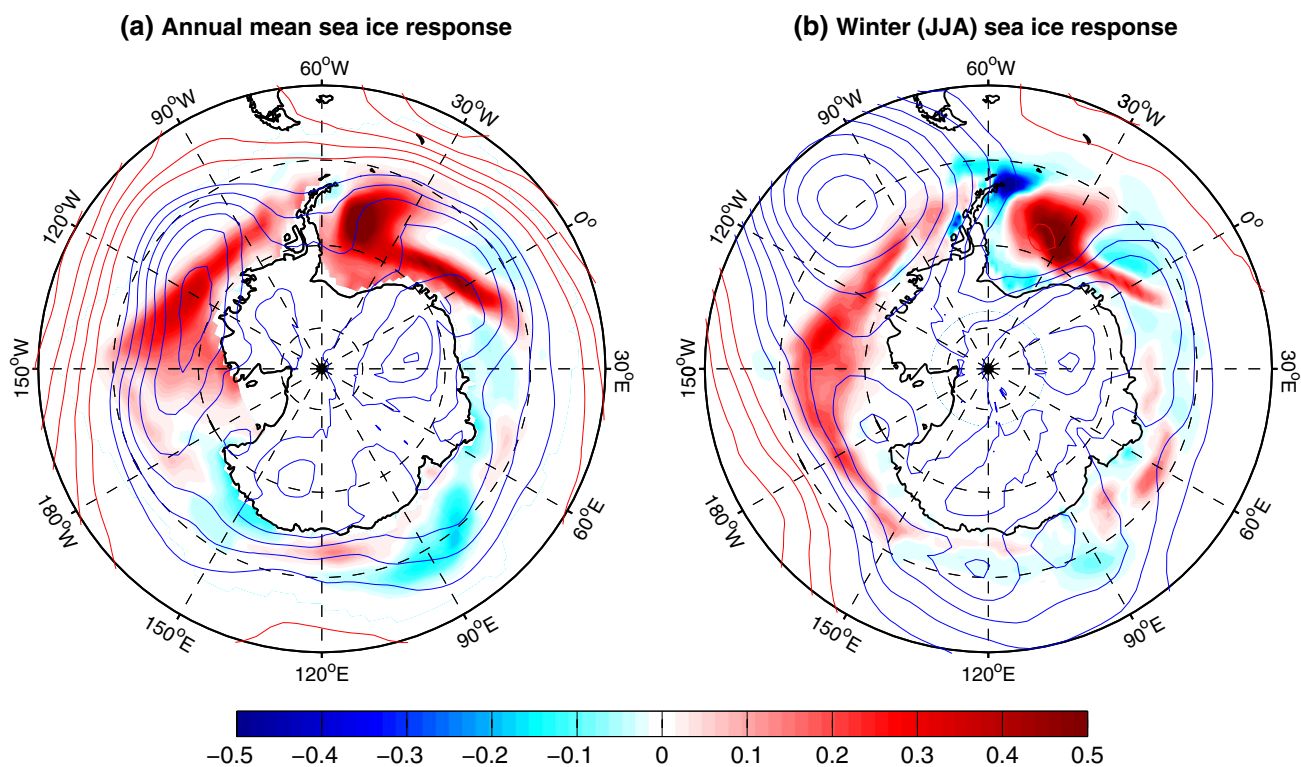


**Fig. 7** Shown are the regressions of **a** annual and **b** austral winter mean sea ice concentration (*shading*)/SLP (*contours*) responses versus the 30-year low pass filtered Southern Ocean (90°S–40°S) area averaged SST index in response to the 100-year periodic NAO forcing.

The results are multiplied by  $-1$ . Units are  $100 \text{ } \%/^{\circ}\text{C}$  for the sea ice concentration and  $\text{hPa}/^{\circ}\text{C}$  for the SLP. The contour interval is  $0.3 \text{ hPa}/^{\circ}\text{C}$  for SLP

anomalous positive NAO flux forcing whose amplitude corresponds to one standard deviation of the NAO time series, is used to further test our hypothesis.

#### 4.1 Implications from the 100-year periodic forcing experiment

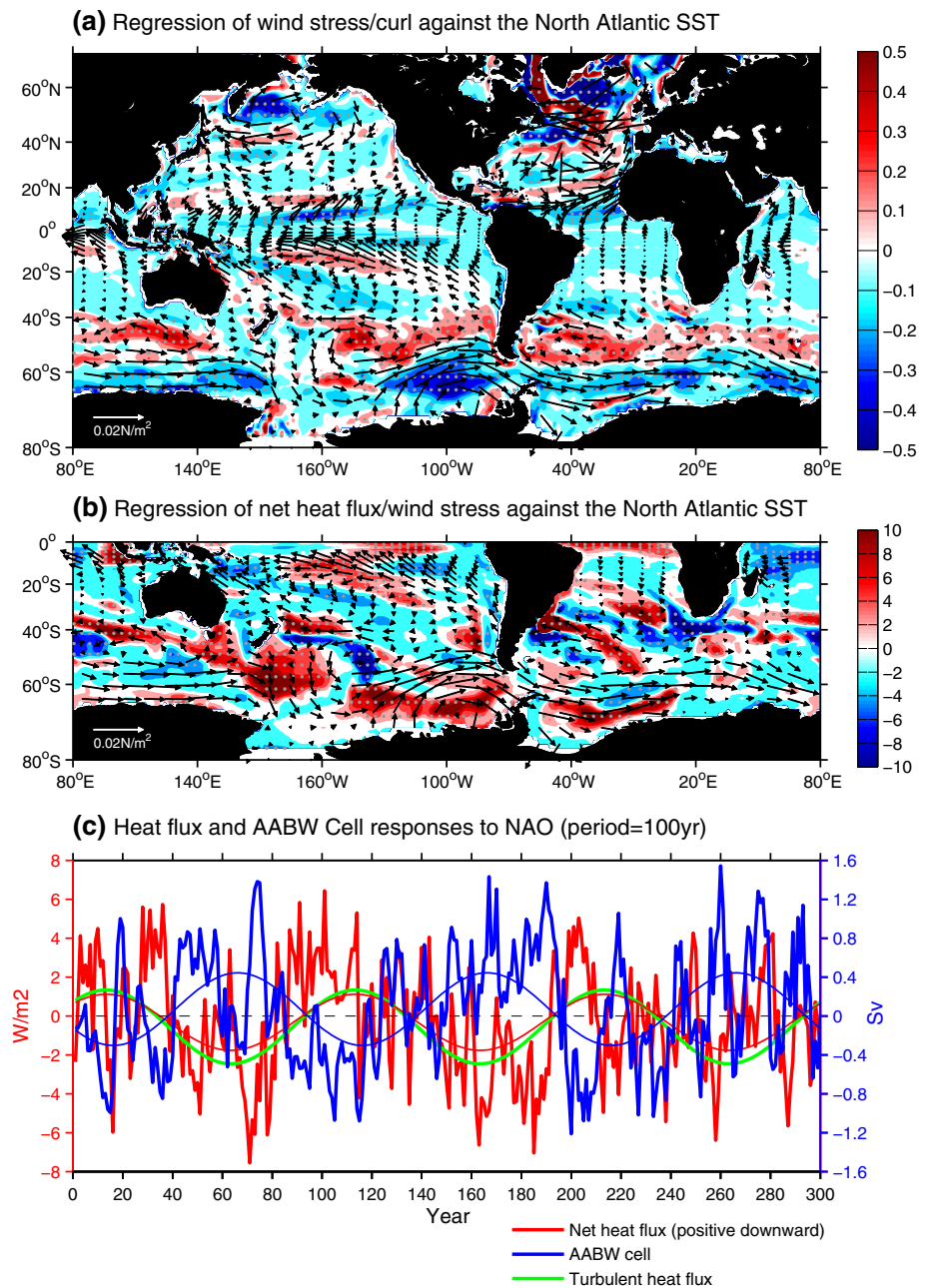
Shown in Fig. 8a are the regressed surface wind stress and wind stress curl anomalies at each grid point versus the area averaged North Atlantic SST time series. The westerly wind over the SO is characterized by a strengthening (weakening) and southward (northward) shift as the North Atlantic warms (cools) generated by the accelerated (decelerated) AMOC. These results suggest that the SO westerly wind anomaly is likely to be a remote response to the anomalous North Atlantic SST induced by the AMOC via atmosphere bridges. This trans-hemispheric atmosphere teleconnection will be verified later.

Consistent with the wind response, the wind stress curl anomaly south of 40°S shows a dipole structure with broad positive values in the north and negative values in the south (Fig. 8a). The positive (negative) wind stress curl over the South Atlantic (40°–60°S) associated with a spin up (down) of AMOC favors a deepening (shoaling) of the isopycnal

depth. By overlapping this wind-driven pycnocline depth anomaly, the  $27.6 \text{ kg}/\text{m}^3$  isopycnal depth shows a much stronger signal over the 40°–60°S band than that in the high latitudinal deep convection region (Weddell sea) where the buoyancy forcing is dominant (Fig. 4).

The westerly wind over the SO further induces surface net heat flux anomalies over the Weddell Sea where the AABW forms. Figure 8b shows that a strengthening and poleward shifted westerly is accompanied with a net heat flux input into the Weddell Sea and vice versa. We note that the long term mean wind stress is a prevailing easterly over the Weddell Sea (Fig. 2c). The anomalous westerly (easterly) wind associated with an accelerated (a decelerated) AMOC weakens (strengthens) the wind speed over the Weddell Sea, reduces (enhances) the turbulent heat loss and therefore warms the ocean. We also show in Fig. 8c the area averaged heat flux over the Weddell Sea and the AABW time series. The net heat flux anomaly contributed mainly from the turbulent heat flux (latent and sensible fluxes) fluctuates almost out of phase with the AABW cell on multidecadal time scales, with a heat flux warming the ocean coinciding with a decelerated AABW Cell and vice versa. This implies that the multidecadal AABW cell fluctuation is likely driven by the local heat flux induced by the westerly

**Fig. 8** **a** Regression coefficients of wind stress (*vector*) and wind stress curl (*shading*) responses versus the 30-year low pass filtered North Atlantic ( $0^{\circ}$ – $70^{\circ}$ N) area averaged SST index in the 100-year periodic NAO forcing experiment. **b** Same as **a** but for the wind stress and surface net heat flux (*positive downward*). Units for the wind stress, wind stress curl and net heat flux are  $\text{N/m}^2/^{\circ}\text{C}$ ,  $10^{-7} \text{ N/m}^3/^{\circ}\text{C}$  and  $\text{W/m}^2/^{\circ}\text{C}$ , respectively. **c** Unfiltered and 30-year low pass filtered time series of Weddell Sea area averaged ( $77^{\circ}\text{S}$ – $65^{\circ}\text{S}$ ,  $60^{\circ}\text{W}$ – $10^{\circ}\text{E}$ ) net heat flux ( $\text{W/m}^2$ ), turbulent heat flux ( $\text{W/m}^2$ ) and the AABW cell ( $\text{Sv}$ ) responses. *Gray points* in **a** and **b** denote that the wind stress curl or heat flux is significant at 90 % confidence level



anomaly. As discussed above, the anomalous westerly is likely triggered by the North Atlantic SST associated with the AMOC variation via atmosphere teleconnection.

#### 4.2 Response to “switch-on” forcing

In order to verify our hypothesis mentioned above, we perform another “switch-on” experiment. In this experiment, we suddenly turn on the extra positive NAO heat flux forcing, at a random point in the control simulation, and leave these fluxes on with constant amplitude corresponding to one standard deviation of the observed NAO time series.

This experiment allows us to understand the spin up process of the climate system in response to an instantaneous imposition of the extra positive NAO heat fluxes. We conduct 10-member ensembles of this “switch-on” setup and each ensemble member integrates forward for 150-year. The ensemble mean difference between the “switch-on” experiment and fully coupled control run is taken as the response.

Shown in Fig. 9a is the time series of AMOC and AABW cell responses to the NAO-related flux forcing. The simulated AMOC adjusts over one decade, increasing in amplitude by several Sverdrups (Sv). This positive AMOC anomaly is largely associated with increased density in the deep

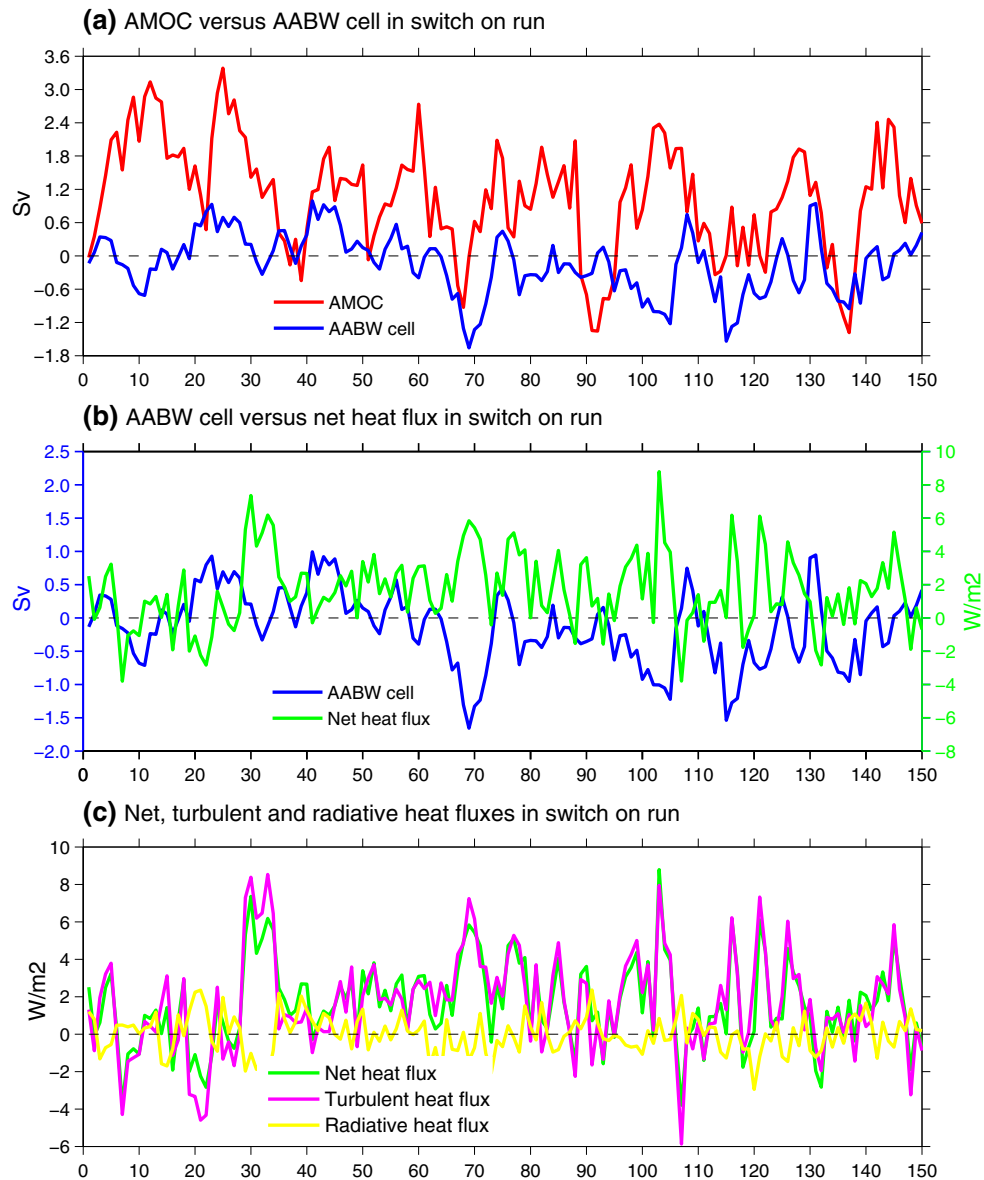


**Fig. 9** Time evolution of various quantities responses to a sudden switch on of heat flux anomaly corresponding to a one standard deviation increase of NAO. **a** AMOC and AABW cell (Sv) responses. **b**

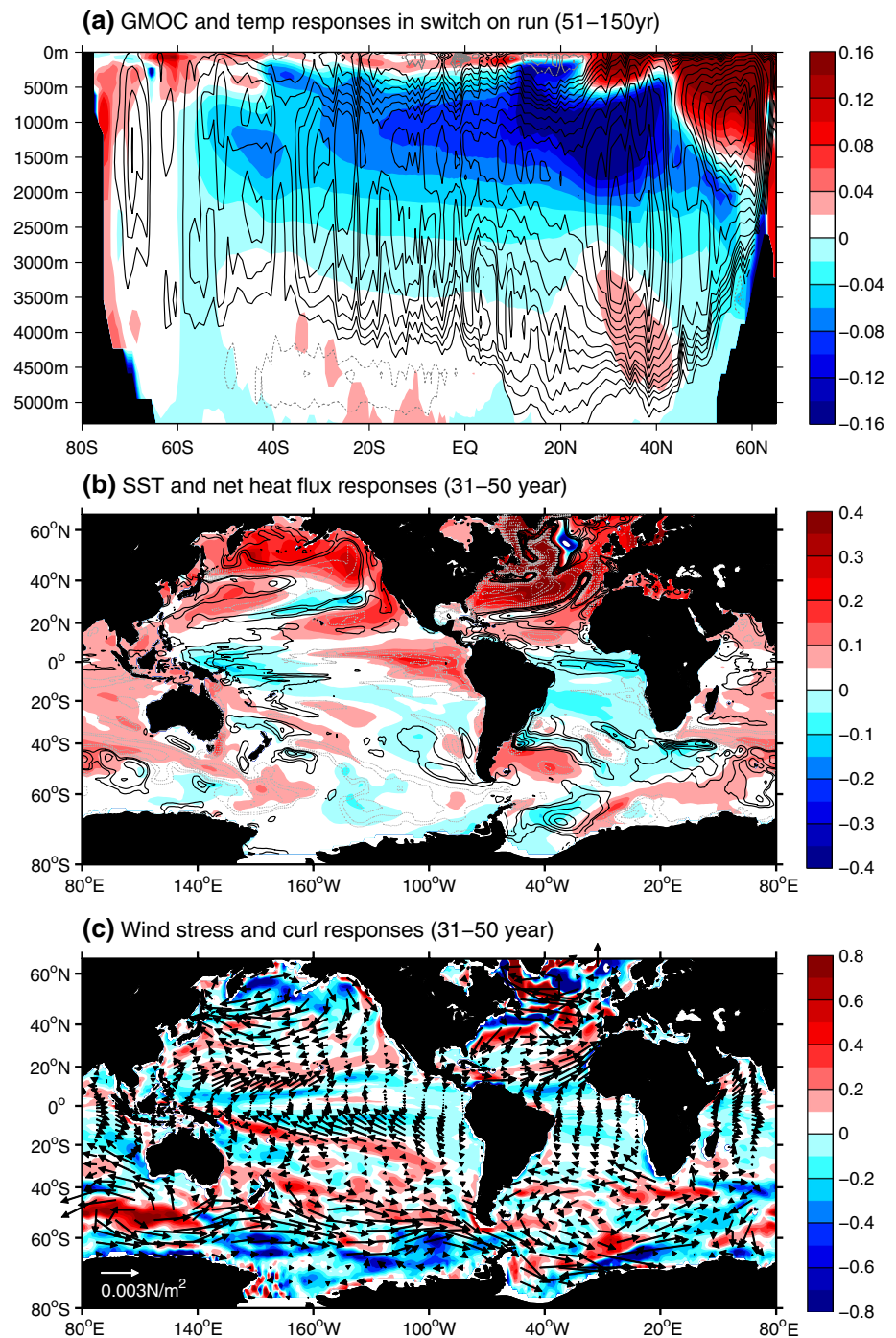
Weddell Sea (77°S–65°S, 60°W–10°E) area averaged net heat flux (W/m<sup>2</sup>) and the AABW cell (Sv) responses. **c** Weddell Sea area averaged net heat flux, turbulent and radiative heat flux (W/m<sup>2</sup>) responses

convection region due to increased surface heat loss during the positive phase of the NAO (e.g. Delworth and Dixon 2000; Delworth and Zeng 2016). As the time integrates forward, the AABW cell gradually weakens. The AABW index is dominated by negative anomalies after about 50 year. This AABW cell decrease is also clearly seen from the last 100 years (year 51–150) of the averaged global meridional overturning streamfunction (GMOC) response (Fig. 10a). The GMOC anomaly exhibits a broad positive value in the upper 4000 m in all latitudes, indicating a strengthened AMOC and a weakened AABW cell. Due to these cell changes, the temperature anomaly features a dipole

structure over both the North Atlantic (warm at the surface, cold in the subsurface) and SO (slight cooling at the surface, warming in the subsurface) south of 60°S (Fig. 10a).

We then examine what processes determine the AABW decrease. As implied by the 100-year periodic NAO forcing experiment, we first investigate the surface heat flux over the Weddell Sea (Fig. 9b). A close inspection finds that the surface net heat flux is dominated by positive anomalies after about 30 years when the AMOC is fully adjusted and the North Atlantic Ocean displays a strong warming (Fig. 10b). It is worth noting that the positive heat flux anomaly leads the AABW cell decrease by several years,

**Fig. 10** Time averaged response to a sudden switch on of heat flux anomaly corresponding to a one standard deviation increase of the NAO. **a** Global meridional overturning circulation (GMOC, contour interval is 0.15 Sv) and Atlantic zonal mean temperature ( $^{\circ}\text{C}$ , shading) responses averaged from year 51 to 150. **b** SST ( $^{\circ}\text{C}$ , shading) and surface net heat flux ( $\text{W}/\text{m}^2$ , contours) responses averaged from year 31 to 50. **c** Wind stress ( $\text{N}/\text{m}^2$ , vector) and wind stress curl ( $\text{N}/\text{m}^3$ , shading) responses averaged from year 31 to 50



indicating that the AABW anomaly is driven by, rather than causes, the surface heat flux change (Fig. 9b). Further decomposition reveals that this anomalous surface net heat flux mainly arises from its turbulent heat flux (latent plus sensible flux), while the contribution from radiative forcing is negligible (Fig. 9c). We also show in Fig. 10b, c the time averaged (year 31–50) surface net heat flux and wind stress responses to the constant NAO forcing. The surface net heat flux over the Weddell Sea tends to warm the ocean;

this is consistent with an anomalous anticlockwise wind in the extratropical South Atlantic, with a weakening of the long term mean easterly over the Weddell Sea (Fig. 10c vs. Fig. 2c). The anomalous anticlockwise wind stress around  $40^{\circ}$ – $60^{\circ}\text{S}$  band corresponds to a positive wind stress curl (Fig. 10c), which favors a deepening of the isopycnal over the extratropical South Atlantic.

We show in Fig. 11 the time evolution of meridional averaged density anomaly in response to a suddenly

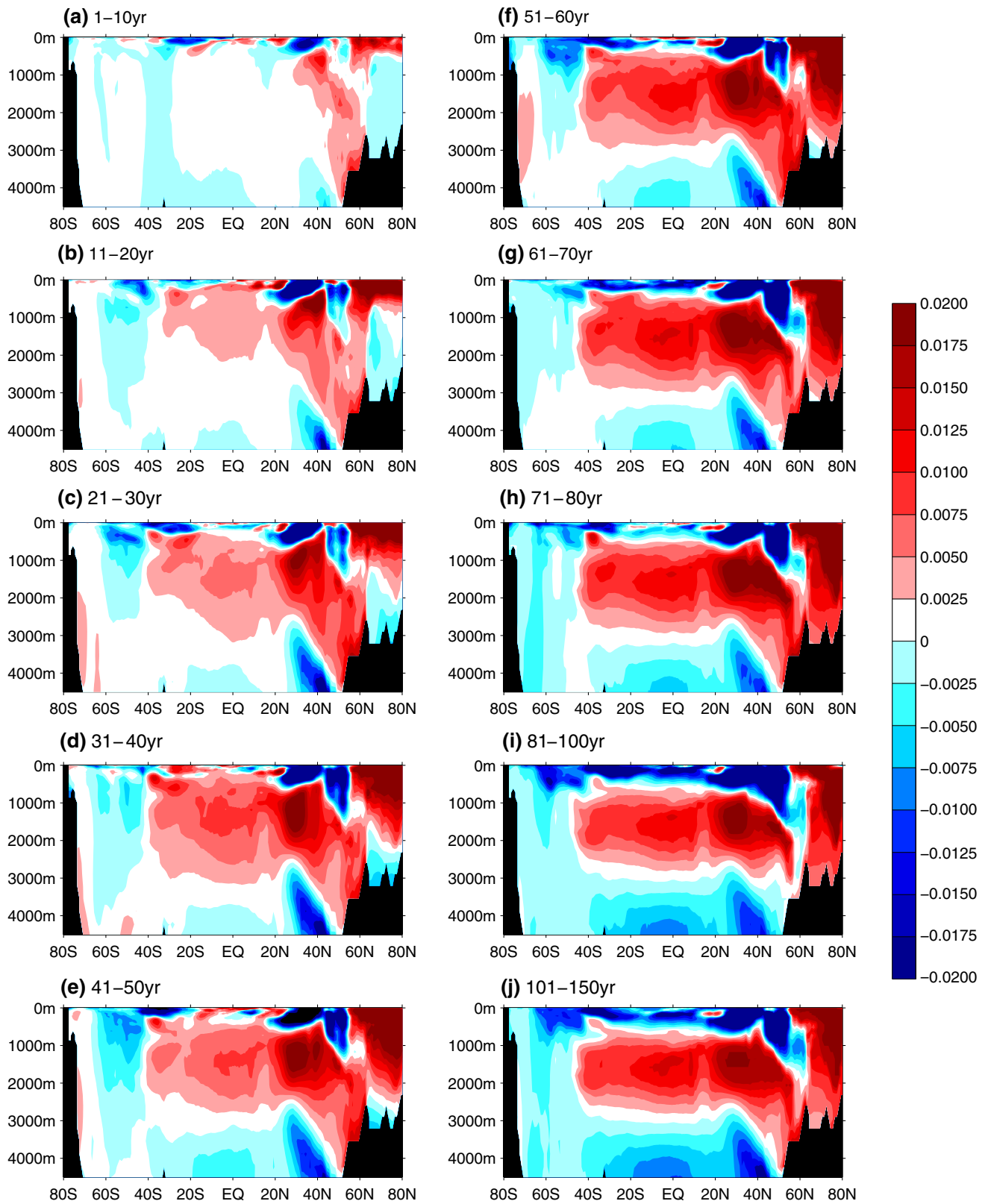


**Fig. 11** Time evolution of Atlantic (80°W–20°E) zonal mean density ( $\text{kg/m}^3$ ) response to a sudden switch on of heat flux anomaly corresponding to a one standard deviation increase of the NAO

imposed NAO forcing. In the first decade, the North Atlantic density increases in both surface and subsurface; this is largely associated with the strengthening of AMOC (Fig. 11a) due to the positive NAO flux forcing. The SO shows no obvious response at this time. From years 11 to 50 the positive density anomaly over the North Atlantic grows and gradually extends southward to the South Atlantic in the subsurface (Fig. 11b–e). This southward penetration is again related to the strengthening of the AMOC. In sharp contrast, there is a density decrease over the SO, which is mainly confined within 40–60°S band (Fig. 11b–e). This negative density anomaly is attributed to the positive wind stress curl shown in Fig. 10c. The positive wind stress curl over the SH favors a surface water convergence, a deepened isopycnal depth, an increased upper ocean heat content and SST (Fig. 10b), and thus a decreased density in a whole column. In the south of 60°S, the density shows a slight increase in the subsurface from year 11 to 50 (Fig. 11b–e). There is a very weak decrease of density in the surface after year 30 (Fig. 11d, e). At year 51–60, the negative density anomaly south of 60°S extends to the upper ocean (Fig. 11f). These density decreases primarily arise from the anomalous surface heating as a result of decreased wind speed over the Weddell Sea (Fig. 10b, c). The decreased density over the SO further grows and progressively penetrates into the deep ocean (Fig. 11g–j), which in turn leads to a weakened AABW cell.

The above suggest that the AABW weakening in response to a strengthened AMOC is largely associated with surface heating over the Weddell Sea as a result of decreased wind speed. Figure 10b, c further shows that this wind speed change over the SO corresponds to a SST warming over the North Atlantic. In the next part, we will use sensitivity experiments to provide further support for this proposed trans-hemispheric atmosphere bridge.

We conduct two parallel experiments to examine whether the AMOC-induced North Atlantic SST anomaly is responsible for driving the SO variability. In the first run, we restore the SSTs in the North Atlantic (0°N–70°N, coast to coast) to their climatological seasonal cycle with a restoring time scale of 5 days, while elsewhere the ocean and atmosphere are fully coupled. The second run is configured the same as the first run, except that the SSTs in the North Atlantic are restored to their climatological seasonal cycle plus the AMOC-induced North Atlantic SST (0°N–70°N) anomaly shown in Fig. 10b. The difference between the first run and the second run is taken as the climate response to the anomalous North Atlantic SST anomaly and named as “Restore\_NASST”. A 10-member ensemble experiment is performed with each experiment starting from widely separated states of the model’s control simulation. Each member runs for 50 years and the last 40-year ensemble means are taken as the equilibrium response.

We show in Fig. 12a the SST and SLP responses in experiment “Restore\_NASST”. The SO generally exhibits a cold SST anomaly. The overlying atmosphere is characterized by a positive phase of SAM, with a high pressure cap surrounded the polar region and a low pressure in the mid-latitude. This anomalous SLP response corresponds to a strengthening and southward shift of the westerly, which could generate anomalous northward Ekman transport, a weakened AABW cell and subsequent SST cooling. We also note that the high SLP over the extratropical South Atlantic (around 40°S–60°S) can induce a surface water convergence, which is accompanied with a deepening of the subsurface isopycnal depth, an increased upper ocean heat content and a warm SST anomaly.

To elucidate how the North Atlantic SST warming drives the SO westerly anomaly, we show the vertical structures of global air temperature changes (Fig. 12b). Significant, broad warming is found in the NH from the surface to the upper atmosphere. There is an exception in the low stratosphere, where cooling occurs. The NH warming tends to penetrate south upward into the tropical upper troposphere. This amplified tropical upper tropospheric warming is largely due to increased latent heat release through enhanced moist convection. In the SH, a weak warming is exhibited in the low and middle troposphere at middle

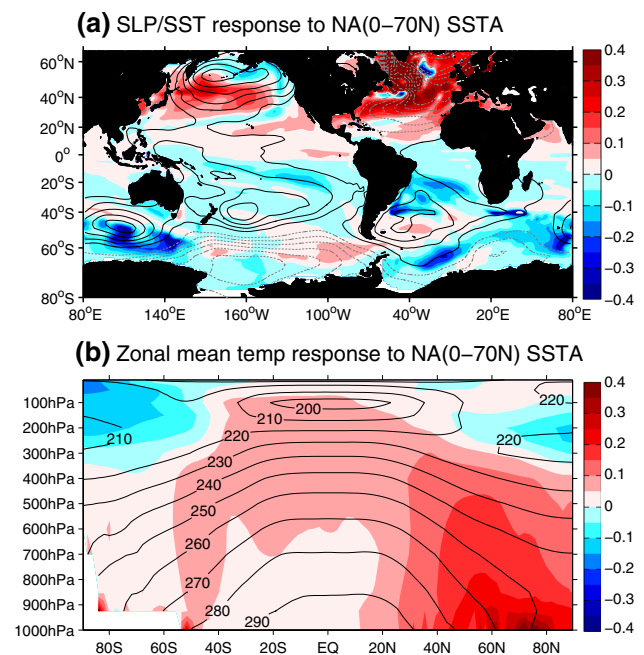


**Fig. 12** **a** Annually-averaged SST ( $^{\circ}\text{C}$ , shading) and SLP (hPa, contour interval: 0.06 hPa) responses in “Restore\_NASST” run in which we impose a North Atlantic (0°–70°N, coast to coast) SST warming anomaly in the coupled model. **b** Zonal mean (0°E–0°W) troposphere temperature (K, shading) response to the anomalous North Atlantic SST warming. The black contours overlapped in **b** denote the long-term mean zonal mean temperature (K)

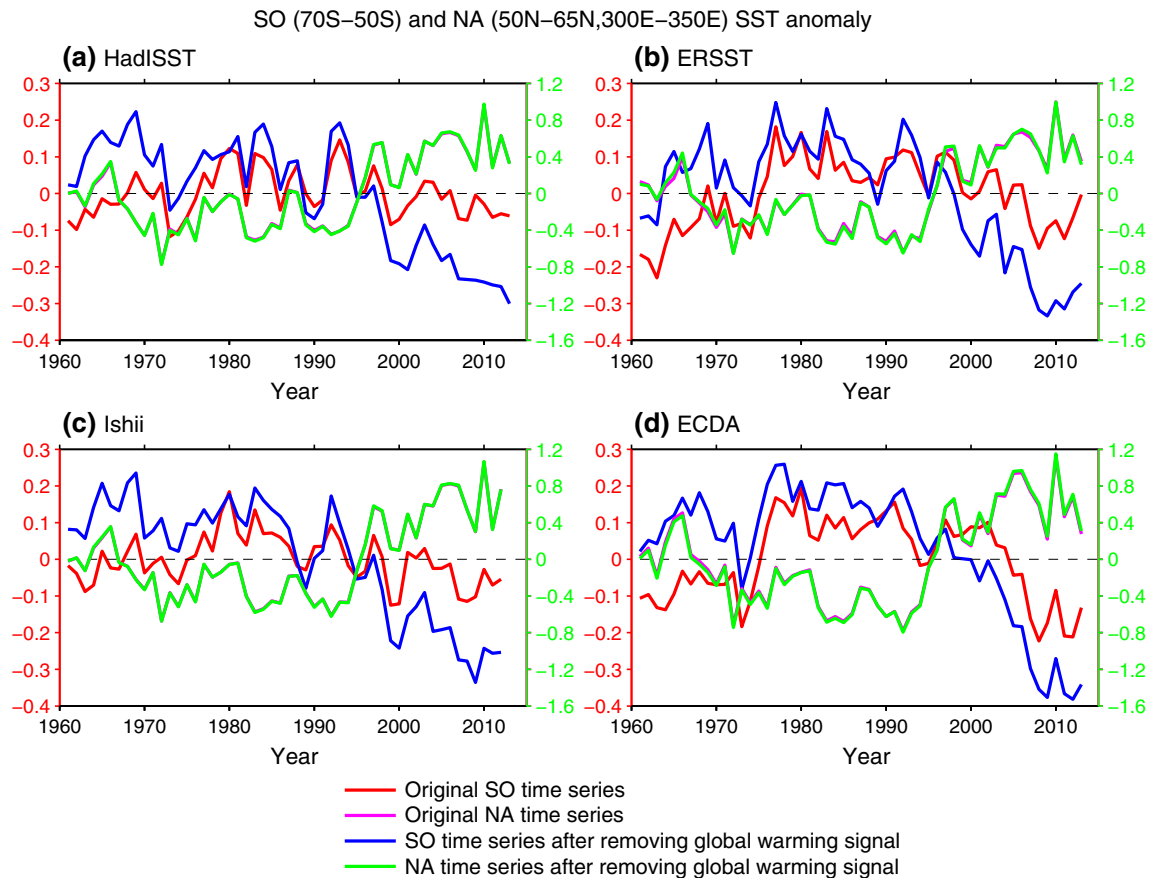


**Fig. 13** Time series of annually-averaged Southern Ocean ( $0^{\circ}$ – $360^{\circ}$ E,  $70^{\circ}$ – $50^{\circ}$ S) and extratropical North Atlantic ( $300^{\circ}$ – $350^{\circ}$ E,  $50^{\circ}$ – $65^{\circ}$ N) area averaged SST ( $^{\circ}$ C) anomaly from 1961 to 2013 in **a** HadISST (Rayner et al. 2003), **b** ERSST (Smith and Reynolds 2004), **c** Ishii (Ishii et al. 2006), and **d** ECDA (Zhang et al. 2007). The anomaly is derived by subtracting the mean value in period 1961–

2013. The red and blue lines denote the original and internal SST variations in the Southern Ocean, with their magnitudes denoted in the left side of y-axis. The magenta and green lines denote the original and internal SST variations in the extratropical North Atlantic, with their magnitudes denoted in the right side of y-axis. Note that the magenta and green lines are overlapped together

and high latitudes, whereas a broad cooling appears above 350 hPa at high latitudes. These temperature features in the SH suggest an increased static stability in the SH mid-latitudes and an increased equator-to-pole temperature gradient in the SH upper troposphere and lower stratosphere, which could favor a poleward shift and strengthening of the westerly jet. Here, the atmosphere bridge from the North Atlantic to the SO is consistent with the findings by Li et al. (2014) and Wang et al. (2015).

### 5 Is the recent SO variation tied to AMOC change?

Over the past few years, most regions in the earth have shown considerable temperature increase in response to greenhouse gas emissions (e.g. Vecchi et al. 2008; Zhang et al. 2011). However, the SO has cooled. Figure 13 exhibits the area averaged SO SST anomaly from 1961

to 2013 in four independent datasets including HadISST, ERSST, Ishii and ECDA reanalysis. The extratropical North Atlantic SST time series is also displayed for comparison. All data show a consistent decreasing trend of SO SST after 1979 especially after 2000 when the cooling SST predominates, while SST anomalies over the extratropical North Atlantic exhibit a significant increase. Here, we use the signal-to-noise maximizing Empirical Orthogonal Function (S/N EOF) (e.g. Ting et al. 2009) to separate the internal variability and external forced response in the SST field. Given that the ECDA reanalysis is based on GFDL CM2.1, we choose the first S/N EOF mode derived from ten members of GFDL CM2.1 historical run as the forced SST response in four datasets for consistency. The forced SST signal is then derived by projecting the area averaged SST anomaly onto the first principal component (PC1). The residual between the original SST time series and the forced SST signal is referred to as the internal variability, which is also shown

## SST difference between 1996–2013 and 1979–1995

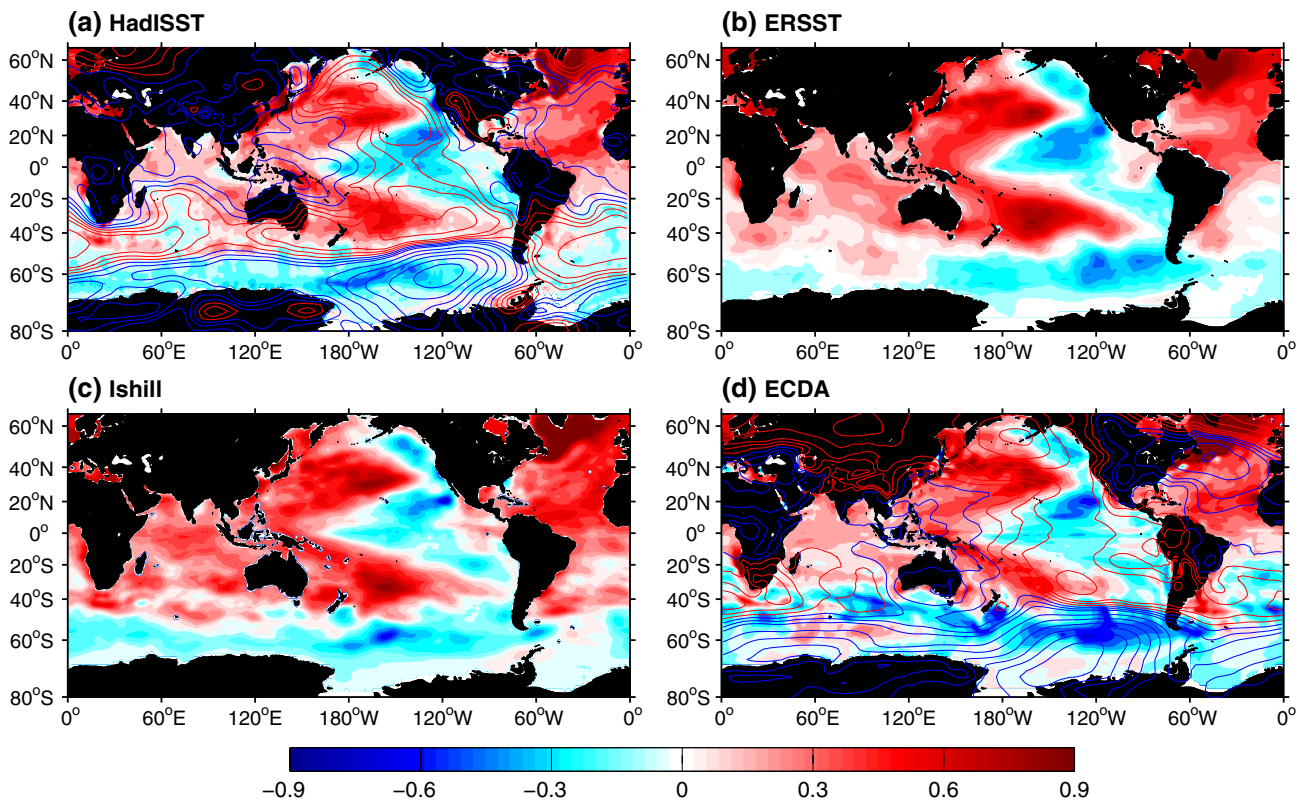


**Fig. 14** Annually-averaged SST(°C) and SLP(hPa) differences between period 1996–2013 and 1979–1995 in **a** HadISST/20CRv2, **b** ERSST, **c** Ishii and **d** ECDA datasets. Contour interval is 0.4 hPa for SLP

in Fig. 13. It can be seen that the original and internal variability of extratropical North Atlantic time series are overlapped together. This implies that the extratropical North Atlantic SST variability is completely driven by the internal variability over the North Atlantic where the AMOC variation dominates. The internal variability of SO SST has the same sign with the original time series but has a much larger amplitude, particularly after 2000, indicating that the external forcing tends to offset but is not a primary factor to determine the SO SST. Moreover, the internal variability of SO SST is negatively correlated with the extratropical North Atlantic SST (or the AMO index), with a warming anomaly in period 1965–1995 and a significant cooling after 1995. This out of phase relationship shares great similarities with the bipolar SST seesaw induced by the multidecadal AMOC variations (Fig. 6), suggesting that the AMOC may play an important role in the recent SO SST change.

To clearly show the spatial structure of SO SST change, we calculate a SST field difference between period 1996–2013 and 1979–1995, as displayed in Fig. 14a–d. Consistent with area averaged anomalies, the SST features a broad cooling over the SO, with large values over

the Pacific and Atlantic basins (Fig. 13 vs. Fig. 14). The atmosphere exhibits a low pressure overlying the cooling SST (Fig. 14a, d), indicating a poleward shift and enhancement of the westerly. Note that the SST outside the SO region also shows significant changes, which resembles the positive phase of AMO (Fig. 14a–d). As discussed in Sect. 4, the Atlantic (0°–70°N) SST warming favors producing a low pressure system over the SO via fast atmosphere bridges. This implies that the recent SO SST change may be attributed, at least partially, to the North Atlantic SST where the internal AMOC variability cannot be negligible.

In contrast to the surface cooling, the subsurface SO shows a significant warming in recent decades (Fig. 15). Both the Ishii data and ECDA reanalysis exhibit an accelerated column averaged warming in the SO subsurface after 2000, albeit with some differences on interannual time scale (Fig. 15a, b). These inconsistencies may arise from the paucity of observations in the SO as well as the model uncertainty. The zonal mean SO temperature difference between period 1996–2013 and 1979–2005 further verifies this surface–subsurface temperature dipole (Fig. 15c, d). This vertical temperature structure in the SO implies



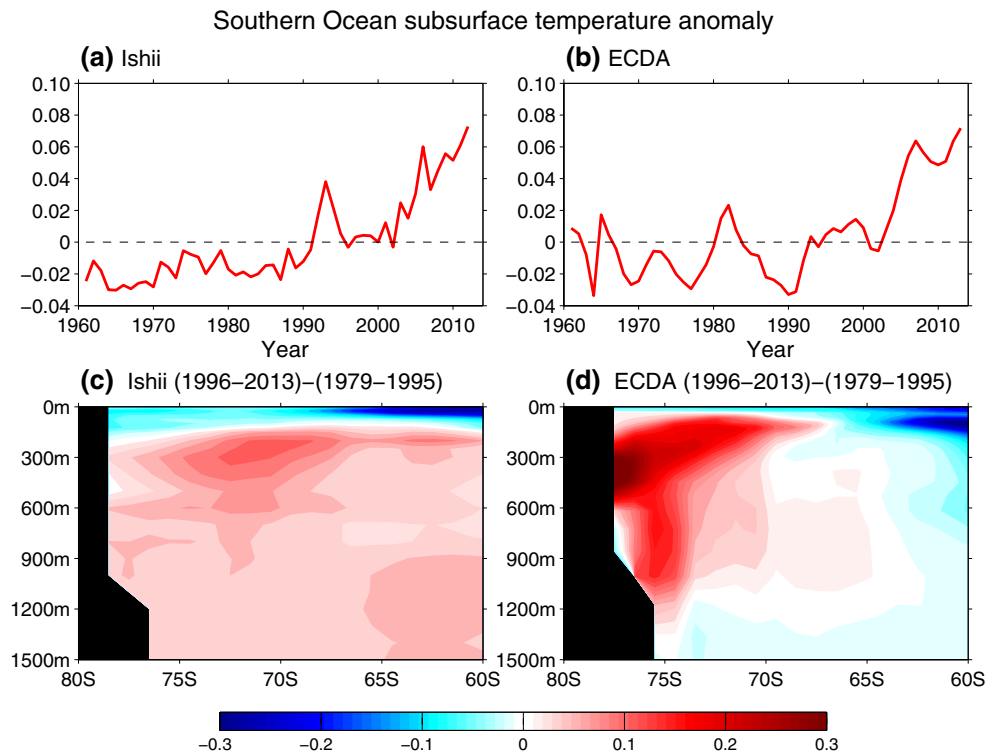


**Fig. 15** Annually-averaged Southern Ocean column averaged ( $0^{\circ}$ – $360^{\circ}$ E,  $90^{\circ}$ – $60^{\circ}$ S, 200–1500 m) subsurface temperature anomaly in **a** Ishii and **b** ECDA data from 1961 to 2013. The anomaly is derived by subtracting the mean value in period 1961–2013. Latitude-depth

section of the zonal mean ( $0^{\circ}$ – $360^{\circ}$ E) temperature difference between 1996–2013 and 1979–1995 in **c** Ishii and **d** ECDA reanalysis. Unit is  $^{\circ}$ C

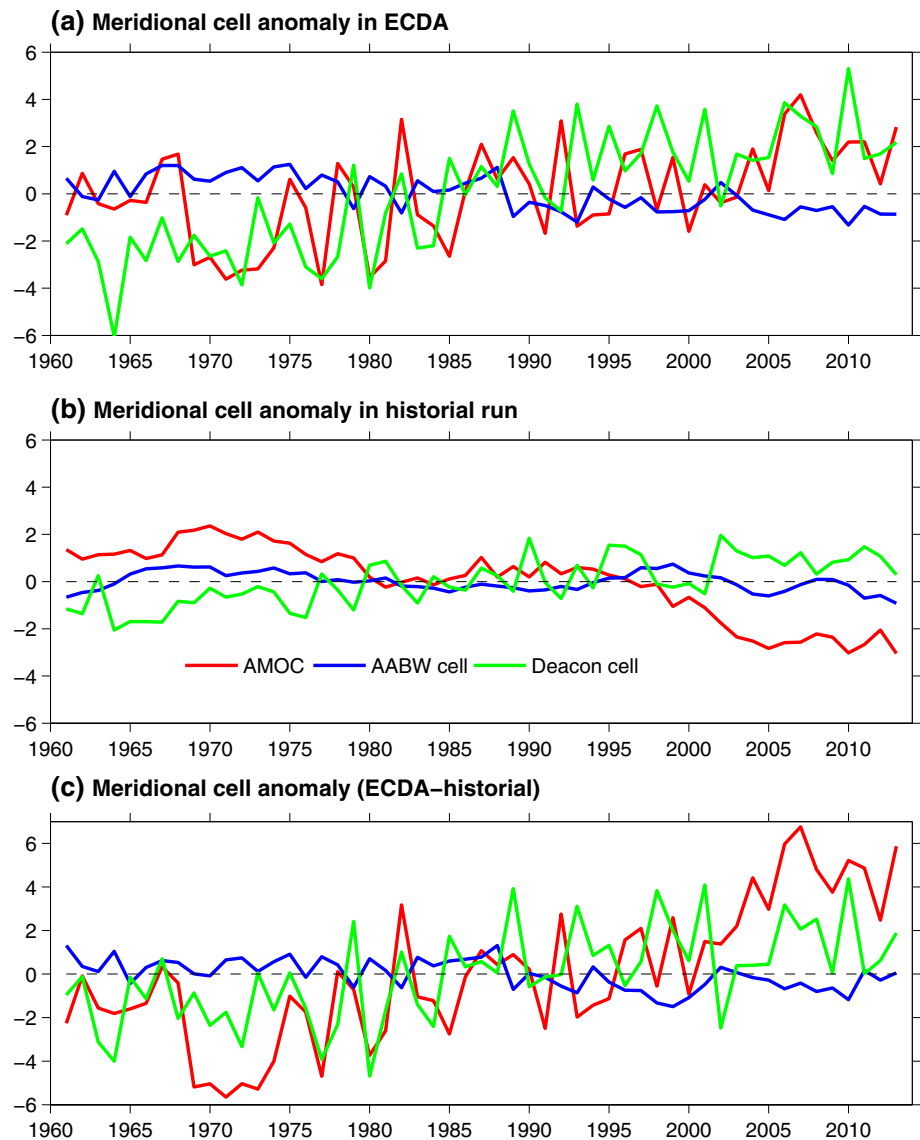
that the AABW formation is weakened in the past few years. To investigate this hypothesis, we plot the AABW, AMOC and Deacon Cell time series in ECDA reanalysis. Here, the MOC definition is based on streamfunction (Fig. 2b), which is the same as that in GFDL CM2.1 model. As presented in Fig. 16a, the AABW cell has a multidecadal fluctuation, with a weakened value after 1990. On the contrary, the AMOC and Deacon Cell are strengthened in the recent two decades. Moreover, these MOC changes are largely attributed to the internal variability (Fig. 16b, c). Figure 16b shows the ensemble mean MOC time series in GFDL historical run, which mainly reflects the effect of external forcing. As expected, both the AMOC and AABW cell are weakened due to the greenhouse gas induced anomalous heating and freshening (e.g. Cheng et al. 2013; Ma and Wu 2011). The Deacon Cell is strengthened under the global warming scenario, which is largely associated with the enhanced westerly as a result of Ozone increase (e.g. Turner et al. 2009). After removing the external forced MOC change, the residual MOC variability still has the same sign with the original time series (Fig. 16a vs. c), indicating a predominant role of internal variability. The SO MOC changes in recent decades are in agreement with their response to the multidecadal AMOC variations

(Fig. 3a). This, again, suggests the potential possibility of AMOC influence on the SO via fast atmosphere bridges and subsequent ocean adjustments.

The sea ice change in recent years is strongly coupled with the SST and surface wind. Figure 17 shows the sea ice difference between period 1996–2013 and 1979–1995 in different seasons. Consistent with Li et al. (2014), the sea ice change during the austral winter (JJA) is characterized by a dipole distribution, with a sea ice increase in the Ross sea, and a broad sea ice decrease in the Amundsen-Bellinghousen-Weddell seas (Fig. 17a). This sea ice dipole is primarily attributed to the Amundsen Sea low induced onshore/offshore air advection as discussed in Sect. 3. During the austral summer (DJF), the sea ice shows a broad increase corresponding to a SST cooling (Fig. 17b). In this season, the ocean temperature becomes a dominant factor to determine the sea ice distribution. The annual mean sea ice change mainly follows the austral winter pattern, albeit with a small amplitude. The dynamical mechanism controlling the sea ice distribution in recent years is generally in agreement with the sea ice response in Fig. 7, which, again, suggests a potential linkage with the AMOC.

Our observational evidences suggest that the SO change has a large possibility to be influenced by the AMOC. This

**Fig. 16** **a** Time series of annually-averaged AMOC, AABW and Deacon Cell anomalies from 1961 to 2013 in ECDA reanalysis. Unit is Sv. **b** Same as **a** but for the ensemble mean results in the GFDL CM2.1 historical run. **c** Difference between **a** and **b**



implies that attributing the recent SO variability should take into consideration not only the local process but also the remote AMOC forcing. While emphasizing the potential role of AMOC in the SO change, we do not wish to down play the potential importance of local circulation and feedbacks in causing the large SO variations such as the internal SO variability independent of AMOC (e.g. Latif et al. 2013).

## 6 Discussion and summary

The impact of multidecadal AMOC variations on the SO is studied in the present paper using the fully coupled GFDL CM2.1 model. It is found that the AMOC can influence the SO via fast atmosphere bridges and subsequent ocean adjustments. A stronger than normal AMOC induces an anomalous warm SST over the North Atlantic, which

favors an increased equator-to-pole temperature gradient in the SH upper troposphere and lower stratosphere due to an amplified tropical upper tropospheric warming as a result of increased latent heat release. This eventually strengthens and pushes the westerly jet poleward. Here, the atmosphere bridge from the North Atlantic to the SO is consistent with the findings by Li et al. (2014) and Wang et al. (2015).

The wind change over the SO then cools the SST by anomalous northward Ekman transports. The wind change also weakens the Antarctic bottom water (AABW) cell through changes in surface heat flux heating forcing. The latter is because the poleward shifted westerly wind decreases the long term mean easterly over the Weddell Sea, reducing the turbulent heat flux loss, decreasing the sea water density and therefore leading to a weakened AABW cell. In the mean state the subsurface is warmer than the surface in the region of the AABW. Therefore, the

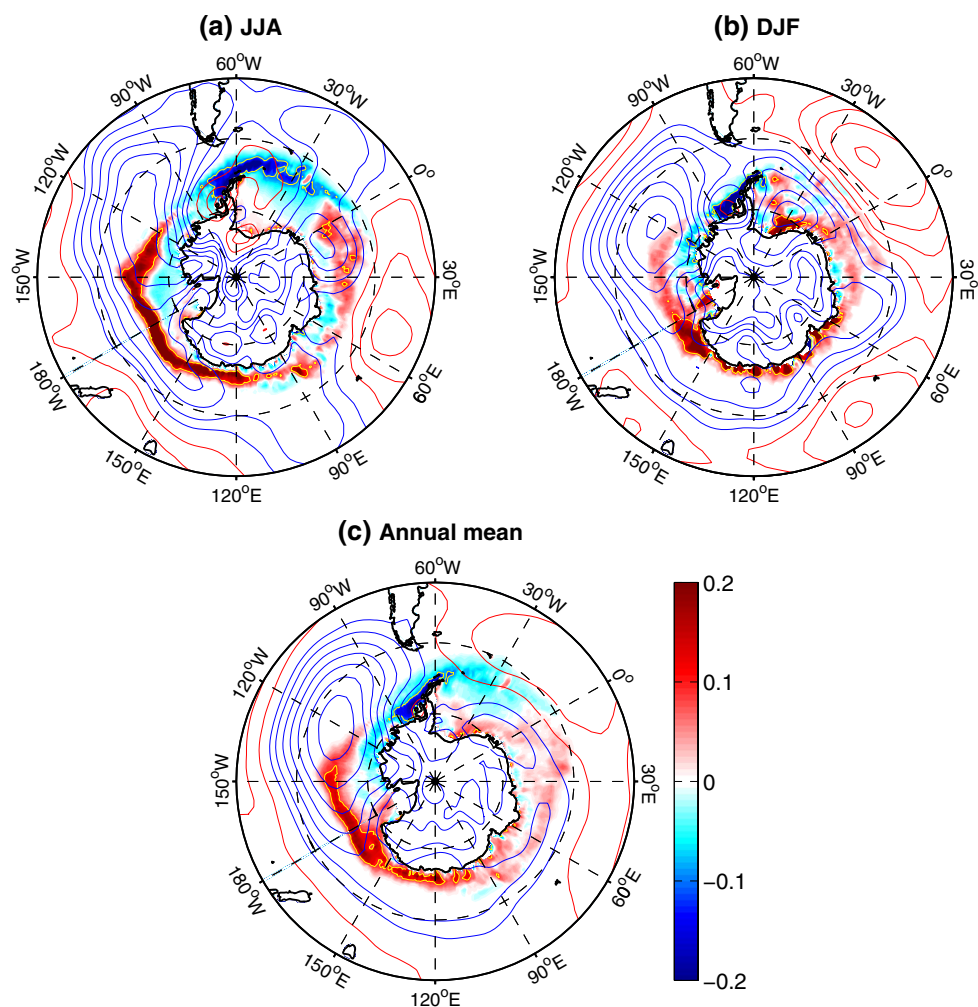


**Fig. 17** Austral winter (a), summer (b) and annual mean (c) sea ice concentration (HadISST) and SLP (20CRv2, contour interval: 0.4) differences between period 1996–2013 and 1979–1995. Units are

100 % for the sea ice and hPa for the SLP. The *yellow contour* indicates the absolute value of sea ice concentration inside is larger than 0.1

spin down of AABW cell drives a surface–subsurface temperature dipole in the SO, with a warming anomaly in the subsurface and a cooling anomaly at the surface that corresponds to an increase of Antarctic sea ice. The SO SST cooling can further feedback to the atmosphere, modestly increasing the westerly winds therefore strengthening the Deacon Cell. The westerly wind response further amplifies the initial SO surface cooling by the enhanced latent heat loss and anomalous northward Ekman transport. Therefore, there is a weak positive air–sea feedback in the SO. The opposite is also true for a weaker than normal AMOC.

The sensitivity of SO response to periodic NAO forcing on time scales ranging from 20 to 200 years is assessed. We see that the model AABW has very little response to forcing at time scales shorter than five decades or so (not shown). The adjustment processes by which the AABW responds to the AMOC and the AMOC responds to the

NAO take of order five decades, so that forcing on shorter timescales is not able to significantly influence the AABW. At longer timescales the AABW varies largely out of phase with the AMOC and NAO forcing, although exhibiting some preference for forcing close to the dominant timescale of SO internal variability (approximately 70–120 years for the GFDL CM2.1 model) (not shown). We note that the 100-year periodic NAO forcing we imposed in the model is close to the internal variability of AABW formation over the SO, thus the SO system is easier to oscillate with large amplitudes and short lags compared to switch on experiment. Although the SO adjustment time scales is different, the associated physical processes in both experiments are the same.

The dynamical linkages between the AMOC and SO have some implications for the recent observed SO change. The SO SST depicts pronounced multidecadal variations

during the instrumental period. During the recent two decades with the advent of satellite, the observations consistently show a cooling SST trend over the SO, while the North Atlantic exhibits a significant warming trend. Moreover, the subsurface SO temperature features a warm anomaly. This surface–subsurface dipole temperature structure implies that the AABW formation is weakened. ECDA reanalysis confirms that the AABW cell does weaken in the past few years, which coincides with a strengthened AMOC. We hypothesize that the remarkable SO SST cooling during the recent decades can be attributed, at least partly, to the AMOC change. We need to keep in mind that the observed multidecadal/trend pattern might be a superposition of several internal modes and externally forced variability. The good correspondence of the observed changes with the model patterns may be thus partly coincidental. Furthermore, the methods used to separate the internal and external variability, such as the S/N EOF used in current paper, are still under debate. More and more direct ocean observation, particularly subsurface observations over the far SO, are needed to better assess the model variability and verify the existence of bipolar ocean seesaw in the real world. Comparison of the AMOC influence on the SO in the GFDL model with that simulated by other climate models will also be helpful.

**Acknowledgments** The authors would like to thank Liwei Jia and Monika Barcikowska for very helpful comments on an earlier version of this manuscript.

## References

- Altabet MA, Higginson MJ, Murray DW (2002) The effect of millennial-scale changes in Arabian Sea denitrification on atmospheric CO<sub>2</sub>. *Nature* 415:159–162
- Black DE, Peterson LC, Overpack JT, Kaplan A, Evans MN, Kshgarian MK (1999) Eight centuries of North Atlantic ocean atmosphere variability. *Science* 286:1709–1713
- Blunier T, Brook EJ (2001) Timing of millennial-scale climate change in Antarctica and Greenland during the last glacial period. *Science* 291:109–112
- Broecker WS (1998) Paleoocean circulation during the last deglaciation: a bipolar seesaw? *Paleoceanography* 13:119–121
- Broecker WS (2000) Was a change in thermohaline circulation responsible for the Little Ice Age? *Proc Natl Acad Sci* 97:1339–1342
- Bryden H, Longworth HR, Cunningham SA (2005) Slowing of the Atlantic meridional overturning circulation at 25°N. *Nature* 438:655–657
- Cheng W, Chiang JCH, Zhang D (2013) Atlantic meridional overturning circulation (AMOC) in CMIP5 models: RCP and historical simulations. *J Clim* 26:7187–7197
- Compo GP, Whitaker JS, Sardeshmukh PD, Matsui N, Allan BJ, Yin X, Gleason BE, Vose RS, Rutledge G (2011) The twentieth century reanalysis project. *Q J Roy Meteorol Soc* 137:1–28
- Crowley TJ (1992) North Atlantic deep water cools the Southern Hemisphere. *Paleoceanography* 7:489–497
- Dee DP et al (2011) The ERA-Interim reanalysis: configuration and performance of the data assimilation system. *Q J Roy Meteorol Soc* 137(656):553–597
- Delworth TL, Dixon KW (2000) Implications of the recent trend in the Arctic/North Atlantic Oscillation for the North Atlantic thermohaline circulation. *J Clim* 13:3721–3727
- Delworth TL, Mann ME (2000) Observed and simulated multidecadal variability in the Northern Hemisphere. *Clim Dyn* 16:661–676
- Delworth TL, Zeng F (2012) Multicentennial variability of the Atlantic meridional overturning circulation and its climatic influence in a 4000 year simulation of the GFDL CM2.1 climate model. *Geophys Res Lett* 39:L13702. doi:10.1029/2012GL052107
- Delworth TL, Zeng F (2016) The impact of the North Atlantic Oscillation on climate through its influence on the Atlantic meridional overturning circulation. *J Clim* 29:941–962
- Delworth TL, Manabe S, Stouffer RJ (1993) Interdecadal variations of the thermohaline circulation in a coupled ocean-atmosphere model. *J Clim* 6:1993–2011
- Delworth TL et al (2006) GFDL's CM2 global coupled climate models. Part I: formulation and simulation characteristics. *J Clim* 19:643–674
- Delworth TL et al (2008) The potential for abrupt change in the Atlantic meridional overturning circulation In: *Abrupt climate change: final report, synthesis & assessment product 3.4*, CSSP, Reston, VA, U.S. Geological Survey, pp 258–359
- Dong BW, Sutton RT (2002) Adjustment of the coupled ocean-atmosphere system to a sudden change in the thermohaline circulation. *Geophys Res Lett* 29:1728
- Dong BW, Sutton RT (2007) Enhancement of ENSO variability by a weakened Atlantic thermohaline circulation in a coupled GCM. *J Clim* 20:4920–4939
- Folland CK, Parker DE, Kates FE (1984) Worldwide marine temperature fluctuations 1856–1981. *Nature* 310:670–673
- Ganachaud A, Wunsch C (2001) Improved estimates of global ocean circulation, heat transport and mixing from hydrographic data. *Nature* 408:453–457
- Gray WM, Sheaffer JD, Landsea CW (1997) Climate trends associated with multidecadal variability of Atlantic hurricane activity. In: Diaz HF, Pulwarty RS (eds) *Hurricanes: climate and socioeconomic impacts*. Springer, New York, pp 15–53
- Hurrell JW (1995) Decadal trends in the North Atlantic Oscillation region temperatures and precipitation. *Science* 269:676–679
- Ishii M, Kimoto M, Sakamoto K, Iwasaki SI (2006) Steric sea level changes estimated from historical ocean subsurface temperature and salinity analyses. *J Oceanogr* 62:155–170
- Johnson HL, Marshall DP (2002) A theory for the surface Atlantic response to thermohaline variability. *J Phys Oceanogr* 32:1121–1132
- Knight JR, Allan RJ, Folland CK, Vellinga M, Mann ME (2005) A signature of persistent natural thermohaline circulation cycles in observed climate. *Geophys Res Lett* 32:L20708. doi:10.1029/2005GL024233
- Latif M, Martin T, Park W (2013) Southern Ocean sector centennial climate variability and recent decadal trends. *J Clim* 26:7767–7782
- Li X, Holland DM, Gerber EP, Yoo C (2014) Impacts of the north and tropical Atlantic Ocean on the Antarctic Peninsula and sea ice. *Nature* 505:538–542
- Lohmann K, Drange H, Bentsen M (2009) Response of the North Atlantic subpolar gyre to persistent North Atlantic oscillation like forcing. *Clim Dyn* 32:273–285
- Ma H, Wu L (2011) Global teleconnections in response to freshening over the Antarctic Ocean. *J Clim* 24:1071–1088
- Martin T, Park W, Latif M (2013) Multi-centennial variability controlled by Southern Ocean convection in the Kiel Climate Model. *Clim Dyn* 40:2005–2022

- Peterson LC, Haug GH, Hughen KA, Rohl U (2000) Rapid changes in the hydrological cycle of the tropical Atlantic during the last glacial. *Science* 290:1947–1951
- Rayner NA, Parker DE, Horton EB, Folland CK, Alexander LV, Rowell DP, Kent EC, Kaplan A (2003) Global analyses of sea surface temperature, sea ice, and night marine air temperature since the late nineteenth century. *J Geophys Res*. doi:10.1029/2000JD002670
- Schmitz WJ (1996) On the world ocean circulation, vol 1. Woods Hole Oceanographic Institute WHOI-96-03, p 141
- Smith TM, Reynolds RW (2004) Improved extended reconstruction of SST. *J Clim* 17:2466–2477
- Stocker TF, Wright DG, Broecker WS (1992) The influence of high-latitude surface forcing on the global thermohaline circulation. *Paleoceanography* 7:529–541
- Stouffer RJ et al (2006) Investigating the causes of the response of the thermohaline circulation to past and future climate changes. *J Clim* 19:1365–1387
- Stouffer RJ, Seidov D, Haupt BJ (2007) Climate response to external sources of freshwater: North Atlantic versus the Southern Ocean. *J Clim* 20:436–448
- Swingedouw D, Fichefet T, Goosse H, Loutre MF (2009) Impact of transient freshwater releases in the Southern Ocean on the AMOC and climate. *Clim Dyn* 33:365–381
- Timmermann AM, An S, Krebs U, Goosse H (2005) ENSO suppression due to a weakening of the North Atlantic thermohaline circulation. *J Clim* 18:3122–3139
- Timmermann AM et al (2007) The influence of a weakening of the Atlantic meridional overturning circulation on ENSO. *J Clim* 20:4899–4919
- Ting M, Kushnir Y, Seager R, Li C (2009) Forced and internal twentieth-century SST trends in the North Atlantic. *J Clim* 22:1469–1481
- Turner J, Comiso JC, Marshall GJ, Lachlan-Cope TA, Bracegirdle T, Maksym T, Meredith MP, Wang Z, Orr A (2009) Non-annular atmospheric circulation change induced by stratospheric ozone depletion and its role in the recent increase of Antarctic sea ice extent. *Geophys Res Lett* 36:L08502. doi:10.1029/2009GL037524
- Vecchi GA, Clement A, Soden BJ (2008) Examining the tropical Pacific's response to global warming. *Eos Trans* 89:81–83
- Vellinga M, Wood R, Gregory JM (2002) Processes governing the recovery of a perturbed thermohaline circulation in HadCM3. *J Clim* 15:764–779
- Wang C, Zhang L (2013) Multidecadal ocean temperature and salinity variability in the tropical North Atlantic: linking with the AMO, AMOC, and subtropical Cell. *J Clim* 26:6137–6162
- Wang YJ, Cheng H, Edwards RL, An ZS, Wu JY, Shen CC, Dorale JA (2001) A high-resolution absolute-dated late Pleistocene monsoon record from Hulu Cave, China. *Science* 294:2345–2348
- Wang XF, Auler AS, Edwards RL, Cheng H, Cristalll PS, Smart PL, Richards DA, Shen CC (2004) Wet periods in northeastern Brazil over the past 210 kyr linked to distant climate anomalies. *Nature* 432:740–743
- Wang Z, Zhang X, Guan Z, Sun B, Yang X, Liu C (2015) An atmospheric origin of the multi-decadal bipolar seesaw. *Sci Rep* 5:8909
- Weaver AJ, Saenko OA, Clark PU, Mitrovica JX (2003) Meltwater pulse 1A from Antarctica as a trigger of the Bølling–Allerød warm interval. *Science* 299:1709–1713
- Wu L, Li C, Yang C, Xie SP (2008) Global teleconnections in response to a shutdown of the Atlantic meridional overturning circulation. *J Clim* 21:3002–3019
- Wunsch C, Heimbach P (2006) Estimated decadal changes in the North Atlantic meridional overturning circulation and heat flux 1993–2004. *J Phys Oceanogr* 36:2012–2024
- Zhang R (2010) Latitudinal dependence of Atlantic meridional overturning circulation (AMOC) variations. *Geophys Res Lett* 37:L16703. doi:10.1029/2010GL044474
- Zhang R, Delworth TL (2005) Simulated tropical response to a substantial weakening of the Atlantic thermohaline circulation. *J Clim* 18:1853–1860
- Zhang L, Wang C (2013) Multidecadal North Atlantic sea surface temperature and Atlantic meridional overturning circulation variability in CMIP5 historical simulations. *J Geophys Res Oceans* 118:5772–5791
- Zhang S, Harrison MJ, Rosati A, Wittenberg A (2007) System design and evaluation of coupled ensemble data assimilation for global oceanic climate studies. *Mon Weather Rev* 135:3541–3564
- Zhang L, Wu L, Yu L (2011) Oceanic origin of a recent La Niña-like trend in the tropical Pacific. *Adv Atmos Sci* 28:1109–1117